Mineralium Deposita
https://doi.org/10.1007/s00126-026-01448-1

ARTICLE

The granite-pegmatite-associated Marvel Loch gold deposit, Yilgarn Craton, Western Australia: magnesian and calcic gold skarns in a 1.5 km long contact zone

Andreas G. Mueller[1]

Received: 22 July 2025 / Accepted: 20 March 2026

Abstract
Marvel Loch (63 t Au) represents a group of high-P (300–400 MPa) gold deposits spatially associated with 2.65–2.62 Ga, garnet-muscovite and spodumene pegmatites in the 3.0 Ga Southern Cross greenstone belt, Yilgarn Craton. The ore bodies terminate at 650–800 m depth at pegmatitic granite. Structural relations, mass-balance calculations, $^{87}Sr/^{86}Sr$ and $^{206}Pb/^{204}Pb$ in scheelite and galena, and the $\delta^{13}C_{PDB}$ of CO_2 (-4.8‰) in the calcite-depositing fluid implicate the I-type granite below as the source. Magnesian olivine-calcite-chlorite-phlogopite, quartz-diopside, and calcic diopside-hornblende skarn (4–15 g/t Au), and low-grade biotite-anorthite-microcline gneiss occur in a 1.5 km long foliated zone bound to the contact meta-komatiite / meta-gabbro. Garnet-biotite and Ti-in-biotite thermometry indicate a peak temperature of 650–550 °C during calcic skarn and biotite-anorthite-microcline replacement in meta-gabbro, and cooling to about 400 °C during retrograde alteration of anorthite to phengite + prehnite + clinozoisite, confirming estimates for magnesian skarn. The fluid (log f_{O2} = -18 bar at 650 °C) became reduced during cooling and progressive replacement, as suggested by Fe^{3+}/Fe_{total} ratios in whole rocks, CH_4 in fluid inclusions, and positive Eu-anomalies in scheelite. At a sulfur fugacity of 10^{-7}-10^{-9} bar, cooling is reflected in pyrrhotite + Ni-loellingite (600–500 °C) in calcite-rich magnesian skarn, arsenopyrite + pyrrhotite + base-metal sulfides ± bismuth (550–400 °C) in quartz-diopside skarn, and retrograde pyrrhotite + pyrite ± marcasite (450–350 °C) in metasomatic gneiss. Marvel Loch is a gold skarn deposit formed at 11–15 km depth in a batholith environment. Reduced tungsten skarns (7–10 km) share the W-Au-As-Bi signature, and the reduction of a magmatic H_2O-CO_2 fluid during cooling and replacement of ferrous or graphitic host rocks.

Keywords Archean · Greenstone · Granite-pegmatite · Gold · Skarn

Introduction

Marvel Loch is the largest deposit (63 t Au; 1907–2012) in the 3.0 Ga Southern Cross greenstone belt of the Archean Yilgarn Craton, Western Australia. Mines in this belt produced more than 360 metric tons of gold (12 Moz; 1888–2024). The deposits, characterized by clinopyroxene-biotite wall-rock alteration (Keats 1991), have been classified as skarns due to the calc-silicate gangue (Mueller 1988; Mueller and Groves 1991). Petrographic, electron microprobe, mineral equilibria, and isotope studies of magnesian Au-Ag skarn in meta-komatiite at Marvel Loch (Mueller 1991; Mueller et al. 1991), and of calcic Au skarn in iron formation at Nevoria (Mueller 1997; Mueller et al. 2004) constrained fluid temperatures to 650–400 °C at lithostatic pressures of 300–400 MPa (3–4 kbar).

Both deposits became part of reviews dedicated to gold skarns (Meinert 1998, 2000), a group distinguished from other classes of skarn deposits (Fe, Cu, Zn-Pb, W, Mo, Sn) by the main economic metal (Smirnov 1976; Einaudi et al. 1981). Meinert (1998) includes Mesozoic to Archean skarns from deeper crustal settings (200–600 MPa), four replacing upper greenschist to amphibolite facies silicate rocks and one replacing marble. In Meinert et al. (2005), "Au skarns in

Editorial handling: B. Lehmann

✉ Andreas G. Mueller
andreas.mueller2@partner.kit.edu

[1] Karlsruhe Institute of Technology, Applied Geosciences, Adenauerring 20b, Karlsruhe D-76131, Germany

Published online: 28 April 2026

regional metamorphic terranes" are regarded as transitional to non-magmatic orogenic deposits, as defined in Groves et al. (1998), because they "share a lack of association with igneous activity". The Nevoria deposit, however, may "represent a true link between typical Phanerozoic pluton-associated Au skarns and Precambrian Au skarns in high-grade metamorphic terranes" (Meinert et al. 2005: 323–324).

A recent study of gold deposits in the Southern Cross Belt has shown that two-mica granite and garnet-muscovite pegmatite occur in about 70% of all mines. Three of the four largest deposits (>1 Moz; Fig. 1a) terminate at depth at pegmatitic granite (Mueller 2025). Clearly, there is a need for large-scale case studies. Since the initial research on magnesian skarn at the SE-end of the Marvel Loch deposit, focussed on underground workings 250 m in length (Mueller 1991), open pit and underground mining exposed the full extent of the 1.5 km long skarn system bound to the contact meta-komatiite / meta-gabbro. Mining ceased in 2012 when thick granitic pegmatites were encountered at 650–800 m depth below all ore bodies (Shenton 2013). In this study, we expand the petrographic, geochemical, and mineralogical database from the magnesian skarns to the amphibolite-hosted East Lode ore body in skarn-banded biotite gneiss, an alteration style not described previously. For the first time, the combined data and new PTX constraints based on East Lode electron probe micro-analyses (EPMA) outline the entire zone of high-T alteration across the ultramafic-mafic contact. The results permit an informed discussion of the

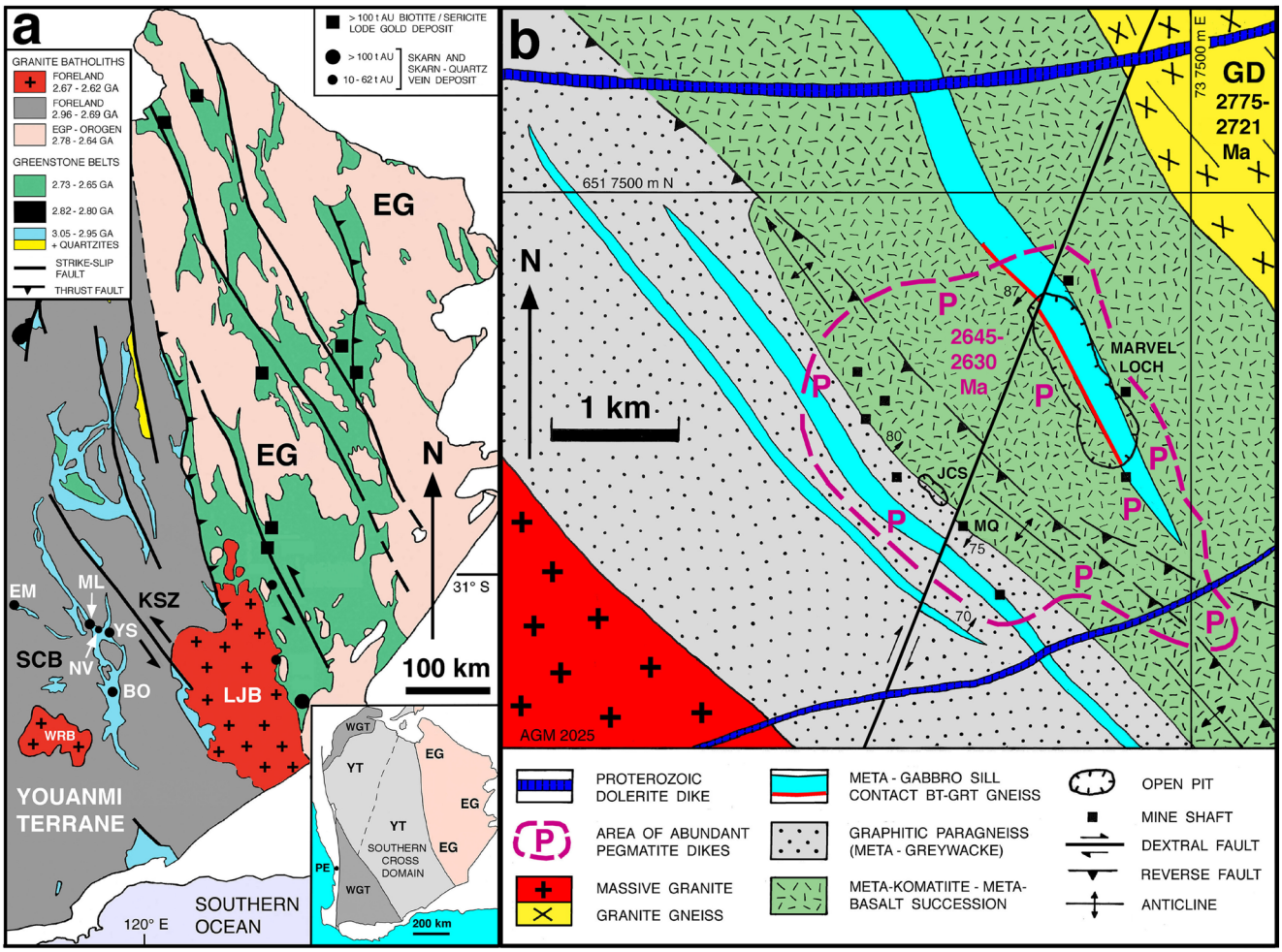

Fig. 1 Regional setting of the 3.0 Ga Southern Cross greenstone belt (SCB), Western Australia. **a** Geologic map of the east Yilgarn Craton (modified from Mueller 2025) showing the 2.7 Ga Eastern Goldfields (EG) orogen and its Youanmi foreland, where post-orogenic I-type granite-pegmatite intrusions peripheral to the Wave Rock (WRB) and Lake Johnston batholiths (LJB) are associated with the Marvel Loch (ML, 63 t Au), Edna May (EM, 46 t Au), Bounty (BO, 41 t Au), Yilgarn Star (YS, 34 t Au) and Nevoria (NV, 18 t Au) skarn deposits, none located in the Koolyanobbing Shear Zone (KSZ). The inset map shows the subdivision of the craton into the EG orogen, the Youanmi Terrane (YT), the Western Gneiss Terranes (WGT), and the city of Perth (PE). Coordinates are latitude and longitude. **b** Geologic map of the Marvel Loch district (modified from Blatchford 1915; Matheson and Hobson 1940) showing the main open pit, and the Mountain Queen (MQ) and Jaccoletti South (JCS) mines. The Ghooli Dome (GD) orthogneiss batholith and massive granite border the greenstones. Coordinates are MGA 1994

magmatic-hydrothermal versus the metamorphic orogenic model, and a comparison of the scheelite-bearing Marvel Loch gold deposit to intrusion-related W-Au skarns.

Terminology and methods

The terms "gneiss" and "schist", usually applied to metamorphic rocks (Bucher and Frey 2002), are used below in the structural sense to describe metasomatic rocks of the East Lode with a widely spaced (biotite-anorthite-microcline gneiss) or closely spaced foliation (almandine-biotite schist). Skarn-banded gneiss contains zones and bands of prograde hornblende and anorthite, and of retrograde clinozoisite and prehnite, calc-silicates common in skarn deposits (Meinert et al. 2005; Table 1). The term "gold skarn" is applied to ore in the sense of Einaudi and Burt (1982), who define the Ca-Mg-Fe-Al silicate gangue "formed by metasomatic processes at relatively high temperature" as the diagnostic feature. The gangue mineralogy specific to endoskarns, and to magnesian or calcic exoskarns is reviewed in the Electronic Supplementary Material (ESM).

Fieldwork began in 1986 during a PhD study (Mueller 1990), and continued intermittently until 2005, when the open pit covered all the historic underground mines on the Undaunted, Exhibition-Firelight, and Marvel Loch leases (Matheson and Hobson 1940; Brabham and Johnson 1995). Notes on mapping and sampling on levels 4–6 of the Marvel Loch shaft, and on the drill holes logged are in the ESM. Samples of metamorphic and altered rocks were stained for K-feldspar, and cut into thin sections, polished thin sections or mounts for examination in transmitted and/or reflected polarized light. Pulverized whole-rock samples were analyzed by X-ray diffraction (XRD) for mineral composition. The major oxides and trace elements were determined by X-ray fluorescence (XRF), by inductive combustion in a Leco furnace, by Mössbauer spectroscopy, by inductively coupled plasma mass spectrometry (ICP-MS), by specific ion electrode (F), by cold vapour atomic absorption spectrometry (Hg), and by fire assay (Au). The analytical details and results are compiled in the ESM. They include the geochemical data of samples taken across an exposure of the East Lode on level 4 of the Marvel Loch shaft (ESM Table 1).

The ESM is also the repository for the methods and data of energy-dispersive electron probe micro-analysis. The EPMA of metamorphic hornblende and plagioclase from meta-gabbro, and of alteration silicates from the East Lode are listed in ESM Tables 2a-e, phlogopite analyses from magnesian skarn in ESM Table 3, gold and loellingite analyses in ESM Table 4, and olivine, spinel and ilmenite analyses from the Savage Lode in ESM Table 5. Silicate names are according to Deer et al. (2013) or according to the nomenclature of the International Mineralogical Association (IMA 1989, 1997, 1998). Endmember compositions are in mole percent (Fo_{80} in olivine). The ratio $Mg/(Mg+Fe^{2+})$ is quoted as the Mg-number in atom percent ($Mg_{49–54}$). Mineral abbreviations are from Whitney and Evans (2010).

The EPMA data tables also list new temperature estimates based on element exchange between mineral pairs using the calibrations of Ferry and Spear (1978), Andersen and Lindsley (1979), Perchuk and Lavrent'eva (1983), and Holland and Blundy (1994). The pre-requisite for such estimates is small-scale equilibrium, deduced from metamorphic or skarn minerals in mutual (non-replacive) contact, as documented in photomicrographs (e.g. Mueller et al. 1991). The results of single-mineral, Ti-in-biotite thermometry according to the empirical calibrations of Henry et al. (2005) and Wu and Chen (2015) are also listed. These thermometers require the co-existence of ilmenite and/or rutile, both present in all rocks of the Marvel Loch deposit. They assume a ratio of $Fe^{3+}/Fe_{total} = 0.12$ in biotite, even in biotite from reduced host rocks. This assumption is supported by the Mössbauer spectroscopy of almandine-biotite schist from the East Lode. Technical aspects of the individual calibrations are reviewed in the ESM.

Regional geology

The Yilgarn Craton has been subdivided based on the stratigraphy and age of its supracrustal belts into the Western Gneiss and the central Youanmi terranes, which constitute the continental foreland of the 2.7 Ga Eastern Goldfields orogen (EG; Fig. 1a). Conglomeratic quartzites containing detrital zircons up to 4.4 Ga old are an integral part of >3.1 Ga para- and orthogneiss belts in the Western Gneiss Terranes. Shelf quartzites also underlie the main 3.0 Ga ultramafic-mafic greenstone succession in the central Youanmi Terrane correlated by a marker horizon of banded iron formation (Watkins and Hickman 1990; Chen et al. 2003; Thern and Nelson 2012).

The 3.0 Ga Southern Cross Belt (SCB) is located in the southeast Youanmi Terrane close to the border with the EG orogen (Fig. 1a). The granitoid batholiths in the area are composed of three generations of orthogneiss dated at ca. 2.96–2.90 Ga, 2.86–2.80 Ga, and 2.78–2.69 Ga. Most of the orthogneiss consists of recrystallized granodiorite and granite associated with minor quartz diorite and trondhjemite-tonalite (Bettenay 1977; Watkins and Hickman 1990). These older intrusions are crosscut by the 2.67–2.62 Ga Wave Rock and Lake Johnston batholiths and their satellite plutons (Fig. 1a). The suite comprises massive I-type granite, lesser granodiorite, and granitic pegmatites with igneous mineralogy and texture. Most plutons are post-orogenic relative to the last folding phases (2665−2655 Ma) in the western part of the EG orogen (Mueller

Table 1 Whole-rock analyses of least-altered metamorphic rocks, magnesian gold skarns, and East Lode gold skarn, gneiss and schist, Marvel Loch deposit, Southern Cross greenstone belt

Rock unit	Metakomatiite	Savage Ld	Boulder Ld	Metagabbro	East Ld	East Ld ore	East Lode
	pillowed	Mg-skarn	Mg-skarn	amphibolite	schist	calcic skarn	gneiss
Assemblage	Hbl-cum-chl	Cal-ol-phl	Qz-di-phl	Hbl-pl ± qz	Alm-bt	Di-hbl-bt	Bt-an-mc
Sample	ML-18	CBSK	Mill head	MLD-8	MLO-64	MLO-68,69	MLO-72
SiO_2 (wt%)	50.21	24.26	56.40	51.14	45.82	52.41	62.02
TiO_2	0.44	0.27	0.33	1.18	1.84	1.10	1.26
Al_2O_3	6.16	4.93	5.73	15.63	18.04	11.22	11.98
Fe_2O_3	0.37	1.99	0.74	0.86	4.22	n.a.	n.a.
FeO	10.93	7.10	6.50	11.65	19.26	11.91	9.86
MnO	0.21	0.17	0.12	0.22	0.31	0.19	0.07
MgO	20.70	18.81	14.57	5.62	2.04	2.91	1.94
CaO	7.04	20.39	7.45	6.68	1.80	7.72	2.63
Na_2O	1.15	< 0.05	0.48	3.56	1.47	0.56	0.13
K_2O	0.04	1.33	1.35	0.38	2.96	2.46	4.88
P_2O_5	0.04	0.03	0.04	0.09	0.19	0.30	0.10
LOI	2.63	18.89	5.27	2.57	2.19	5.96	5.48
Total	99.92	98.17	98.98	99.58	100.14	96.74	100.35
Fe^{3+}/Fe_{Total}	0.03	0.20	0.09	0.06	0.17	n.a.	n.a.
H_2O (wt%)	2.60	3.59	3.19	2.27	2.13	1.08	1.09
CO_2	< 0.05	14.26	1.46	0.18	< 0.05	0.68	< 0.05
S	0.02	1.04	0.62	0.12	0.05	4.20	4.38
Ag (ppm)	**0.08**	5.00	5.70	**0.08**	< 0.10	2.00	0.50
As	**1.90**	3270.00	4539.00	15.00	706.00	3.55%	427.00
Au	0.01	6.42	9.93	< 0.01	0.02	19.37	0.26
Ba	1.80	59.00	118.00	54.00	229.00	179.00	238.00
Be	0.60	0.40	0.70	1.00	0.40	0.70	0.60
Bi	**0.05**	< 0.10	0.47	**0.05**	0.01	0.10	< 0.10
Co	80.00	43.00	46.00	56.00	60.00	32.00	20.00
Cr	2677.00	2341.00	2161.00	104.00	46.00	n.a.	9.00
Cs	0.60	1.90	3.90	0.60	4.10	1.80	1.40
Cu	28.00	30.00	81.00	18.00	16.00	120.00	43.00
F	n.a.	n.a.	155.00	480.00	1150.00	n.a.	n.a.
Ga	4.00	10.00	6.00	22.00	29.00	24.00	17.00
Hg	**0.20**	0.01	0.11	**0.20**	n.a.	0.01	0.05
Li	10.00	7.80	37.00	15.00	26.00	9.10	56.00
Mo	0.50	0.30	2.60	0.50	0.50	0.90	1.10
Nb	3.00	4.00	< 2.00	10.00	11.00	n.a.	10.00
Ni	643.00	716.00	635.00	55.00	287.00	63.00	40.00
Pb	0.80	7.60	130.00	1.60	12.00	8.00	18.00
Rb	0.80	45.00	36.00	12.00	89.00	61.00	90.00
Re	**< 0.01**	n.a.	< 0.01	**< 0.01**	< 0.01	0.40	n.a.
Sb	**1.00**	3.40	22.00	**1.00**	3.90	21.00	< 2.00
Sc	28.00	30.00	22.00	33.00	35.00	n.a.	20.00
Sn	< 0.50	< 0.50	0.70	< 0.50	1.30	0.90	< 0.50
Sr	25.00	304.00	131.00	185.00	54.00	106.00	117.00
Te	**0.01**	< 0.10	0.30	**0.01**	< 0.10	< 0.10	< 0.10
Th	0.40	< 0.10	0.45	2.90	3.30	2.10	2.40
Tl	**0.30**	< 1.00	0.28	**0.30**	0.60	0.33	< 1.00
V	198.00	116.00	145.00	332.00	592.00	279.00	273.00
W	0.90	44.00	48.00	0.50	54.00	1.33%	76.00
Y	10.00	8.00	4.00	29.00	35.00	35.00	29.00
Zn	73.00	76.00	204.00	69.00	101.00	107.00	123.00
Zr (XRF)	27.00	24.00	23.00	105.00	153.00	109.00	110.00
Zr (ICP)	20.00	14.00	13.00	74.00	104.00	87.00	91.00

Table 1 (continued)

Rock unit	Metakomatiite	Savage Ld	Boulder Ld	Metagabbro	East Ld	East Ld ore	East Lode
	pillowed	Mg-skarn	Mg-skarn	amphibolite	schist	calcic skarn	gneiss
Assemblage	Hbl-cum-chl	Cal-ol-phl	Qz-di-phl	Hbl-pl ± qz	Alm-bt	Di-hbl-bt	Bt-an-mc
Sample	ML-18	CBSK	Mill head	MLD-8	MLO-64	MLO-68,69	MLO-72
Rare earth elements (REE)							
La	2.00	1.50	1.69	8.10	12.16	8.40	12.00
Ce	5.10	3.40	3.74	21.00	27.29	19.10	26.00
Pr	1.00	0.60	0.57	2.80	3.54	2.43	3.20
Nd	4.10	2.40	2.54	11.00	16.32	11.40	15.00
Sm	1.00	0.80	0.79	3.00	4.26	3.10	3.40
Eu	0.39	0.30	0.28	1.00	1.36	1.20	1.10
Gd	1.40	1.20	0.92	3.40	4.83	3.91	3.90
Tb	n.a.	n.a.	0.17	n.a.	0.78	0.67	n.a.
Dy	2.00	1.30	1.26	3.50	5.48	5.10	5.00
Er	1.10	0.90	0.72	2.50	3.30	3.03	3.30
Yb	1.10	0.70	0.73	2.00	3.49	2.91	3.00
Lu	0.15	0.10	0.10	0.30	0.54	0.46	0.50
REE total	19.34	13.20	13.51	58.60	83.35	61.71	76.40
Density (g/cc)	3.07	2.93	2.95	2.91	3.23	3.07	2.82

Background values (in bold) for the mantle-derived host rocks are those of basalt in Krauskopf and Bird (1995). Detection limits (DL): XRF oxides 0.01-0.05 wt%, Leco CO2 0.05%, Leco sulfur 0.02%, Loss on ignition (LOI) corrected for oxidation of Fe2, H2O = LOI-CO2-S. XRF trace elements DL 1-7 ppm, ICP-MS 0.01-0.1 ppm (Mueller 1990). Au by fire assay 25 g charge (DL 0.001 ppm), Hg (DL 0.01 ppm), fluorine (DL 50 ppm), n.a. = not analyzed. Pt < 0.1 ppm. ICP data for Hf, Nb, Ta, and U are omitted due to incomplete zircon (and rutile?) dissolution. SAMPLES: ML-18, Marvel Loch shaft 4 level at 9792 m N. CBSK, Savage Lode, 8 samples, 4 level at 9840 m N. Mill head, Boulder Lode, 1735 t of sulfide ore, 4-6 levels. MLD-8, drill core MLD-8, 182 m + ML-4/8, 96 m. MLO-64, 4 level at 9960 m N. MLO-68+69, 2 samples, 4 level at 9960 m N. MLO-72, 4 samples, 6 level at 9870 m N

et al. 2020). The least-evolved members are magnetite-series seriate or K-feldspar megacrystic biotite granites. Fractionated peraluminous members include magnetite- or ilmenite-series pegmatitic granites and Li-Cs-Ta pegmatites (Mueller 2025).

More than 75 per cent of the surface of the Yilgarn Craton is underlain by granite batholiths indicating a deep level of erosion. Late Archean LCT pegmatites characterized by the high-P assemblage spodumene+quartz (300–400 MPa; London 1984) were emplaced at 2650−2620 Ma into all terranes of the craton coeval with gold skarn formation (Mueller 2025; Wells et al. 2025). A lithostatic load of 300–400 MPa corresponds to a depth of 11–15 km based on 3.8 km per 100 MPa for granite density, and 3.6 km per 100 MPa for a mixed granite-greenstone density in the continental crust (Spear 1993).

Southern Cross greenstone belt

The volcanic succession in the SCB comprises a lower unit of tholeiitic amphibolites (>1 km thick) overlain by a horizon (30–60 m) of grunerite-quartz±magnetite banded iron formation (BIF), an upper unit of meta-komatiites (1 km), a second marker horizon (20–40 m) of graphitic schist and chert, and an uppermost unit (0.2 km) of tholeiitic amphibolites. The volcanic rocks are conformably overlain by meta-greywacke (>1 km) composed of graphitic schist and conglomeratic sand-siltstone turbidites. Meta-gabbro sills up to 500 m thick (Willett 1973) and thin sills of quartz porphyry are emplaced into the greenstone-greywacke sequence. The U-Pb zircon age of a porphyry sill sets a minimum of 2934±7 Ma for the succession (Mueller and McNaughton 2000). The BIF horizon outlines regional isoclinal folds refolded during the emplacement of the granitoid batholiths (Mueller et al. 2004).

The greenstones are metamorphosed to amphibolite facies in aureoles contouring the granitoid-greenstone contact (Ahmat 1986). The Marvel Loch, Nevoria and other gold skarn deposits are located in the aureole of the Ghooli Dome orthogneiss batholith (Fig. 1). Steeply plunging mineral lineations and assemblages in the greenstones indicate metamorphism at about 400 MPa during the rise and expansion of the batholith (Dalstra et al. 1998). The U-Pb zircon ages of granitoids in the Ghooli Dome range from 2775−2721 Ma (n=4) in the southeast, and from 2720−2691 Ma (n=5) in the northwest (Doublier et al. 2014). Enclaves of older orthogneiss (2.93–2.92 Ga) occur at two localities (Thebaud et al. 2013a, b). Metamorphic zircons dated at 2772±5 Ma in an altered 2.91 Ga quartz porphyry sill link aureole metamorphism to early pluton emplacement (Mueller and McNaughton 2000), up to 140 Ma before skarn formation at Nevoria (2635.7±1.2 Ma; Mueller et al. 2004).

I-type granites of the 2.67–2.62 Ga suite form a broad plutonic arc at the western margin of the SCB marked by scattered enclaves of greenstone and orthogneiss. Satellite intrusions of two-mica granite and garnet-muscovite pegmatite are spatially associated with gold skarn deposits such

as Marvel Loch (Fig. 1b). The intrusive suite includes Li-Cs-Ta pegmatites at Split Rocks (11.9 Mt at 0.72% Li_2O) close to the Olga group of gold deposits, and the Earl Grey spodumene pegmatite (189 Mt at 1.5% Li_2O) west of the BIF-hosted Bounty gold skarn. The gold and lithium deposits are broadly coeval (Mueller 2025).

Mylonites of the NW-striking Koolyanobbing Shear Zone (KSZ; Fig. 1a), the principal fault with sinistral strike-slip (Libby et al. 1991), are crosscut by massive biotite granite dated at 2656±3 Ma (Qiu et al. 1999). The KSZ is crustal-scale but does not contain gold deposits. It is offset by two sets of faults: (1) NE- to NNE-striking dextral faults with up to 1.5 km displacement and, (2) younger E- to ENE-striking sinistral faults with a south-side-down component of movement. At Nevoria, these faults control barren sericite-chlorite-carbonate alteration in amphibolite (Mueller 1997). They are younger than 2634±4 Ma, as they offset the Nevoria pegmatite-granite pluton. East-trending dikes of norite, dolerite, and nepheline syenite (Ellis 1939), most part of the 2.4 Ga Widgiemooltha suite (Hallberg 1987), postdate all other structures (Fig. 1b).

Marvel Loch mining district

Production at Marvel Loch comprises: (1) intermittent underground mining (0.621 Mt at 7.37 g/t Au; 1907–1991), (2) open pit mining (21 Mt at 1.85 g/t Au; 1984–2005), and (3) underground stoping of bulk ore (6.1 Mt at 3.23 g/t Au recovered; 2005–2012). The ore zone is controlled by the vertical contact of a meta-gabbro sill emplaced into meta-komatiites, the ultramafic volcanic succession overlying the BIF marker horizon at Nevoria (Mueller 1997, 2026). The sill is up to 250 m thick at the open pit, pinches out to the southeast (Fig. 1b) but thickens to the northwest. Layers of meta-pyroxenite and -harzburgite (?) at the northeast contact indicate that the sill faces southwest. Small ore bodies (4,000 t at 16.6 g/t Au) were mined at the ultramafic base of the meta-gabbro (Matheson and Hobson 1940; Keats 1991).

The Marvel Loch deposit is located in the metamorphic aureole of the Ghooli Dome batholith 1.5 km southwest of the orthogneiss contact (Fig. 1b). Least-altered meta-gabbro (Table 1) in the NE-wall of the open pit consists of hornblende ($Mg_{49–54}$; 50 vol%), plagioclase (An30), quartz (3–5%), cummingtonite (3%), and apatite and ilmenite (0.5-1%). The microprobe analyses of metamorphic hornblende-plagioclase pairs and the exchange reactions calibrated by Holland and Blundy (1994) result in a temperature estimate of 650±50 °C (ESM Table 2a).

The komatiite succession in the southwest wall is composed of pillowed meta-pyroxenite (21–26 wt% MgO; Ellis 1939; Mueller 1991), intercalated thin flows of peridotitic meta-komatite (37% MgO), minor high-Mg amphibolite (<18% MgO anhydrous), and interflow beds of graphitic quartz-mica-andalusite schist. The pillowed pyroxenites (Table 1) are metamorphosed to edenite+Mg-hornblende (Mg_{80}), cummingtonite (30–50 vol%), Mg-chlorite (20–30%), ilmenite and chromite (0.5%). Unstrained peridotitic komatiite has a metamorphic texture defined by randomly oriented olivine blades set in a matrix of talc, cummingtonite, and chlorite (Mueller et al. 1991). In some samples (ESM), the metamorphic assemblage talc+chlorite+anthophyllite+tremolite was detected by XRD interstitial to olivine consistent with a peak aureole temperature of about 650 °C (Bucher and Frey 2002).

The contact of the ultramafic rocks with the younger meta-greywacke is conformable. Biotite paragneiss (meta-turbidite) is interbedded with graphitic quartz-mica schist marked by andalusite, staurolite, and almandine porphyroblasts (Matheson and Hobson 1940). Two units of intercalated amphibolite are interpreted as sills (Fig. 1b). Residual metamorphic minerals in soil overlying meta-greywacke are andalusite, minor sillimanite, staurolite, and rare kyanite and Fe-Mg spinel (Carroll 1939). The assemblages almandine+biotite, almandine+staurolite, andalusite+sillimanite, and the rare occurrence of kyanite indicate PT-conditions of about 400 MPa and 550 °C (Fig. 2).

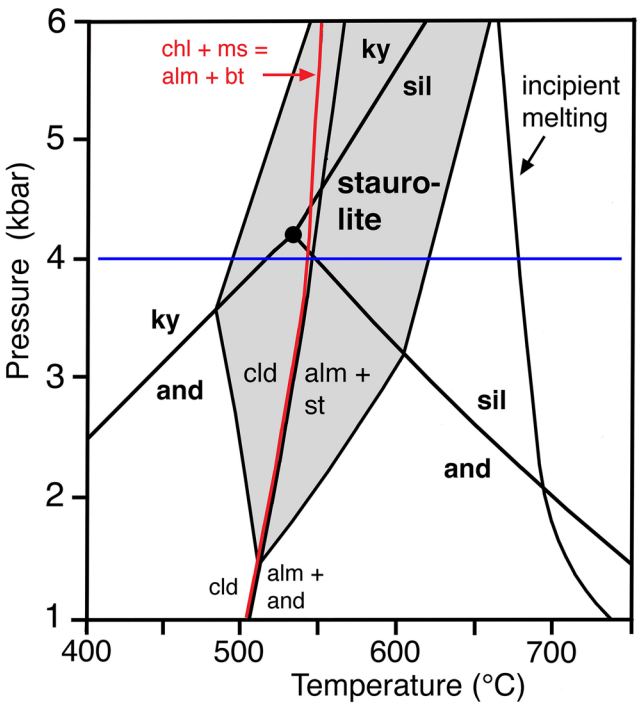

Fig. 2 Pressure-temperature diagram for the KFASH system (modified from Bucher and Frey 2002) showing the phase relations of the Al_2SiO_5 polymorphs (Bohlen et al. 1991), and the metamorphic dehydration reactions in greywacke of the Marvel Loch district (Fig. 1b). The assemblages staurolite+quartz (grey), almandine+staurolite, almandine+biotite and andalusite+sillimanite (+rare kyanite) constrain PT-conditions in the greywacke to about 400 MPa (4 kbar) and 550 °C. Almandine (alm), andalusite (and), biotite (bt), chlorite (chl), chloritoid (cld), kyanite (ky), muscovite (ms), sillimanite (sil), staurolite (st).

The contact meta-greywacke-komatiite about 2.5 km southwest of the Ghooli Dome controls a second line of gold deposits. Lithologic contacts are steeply dipping to vertical (Fig. 1b). The main mines are the Mountain Queen (107,256 t at 8.62 g/t; Matheson and Hobson 1940), Jaccoletti-Comet (34,630 t at 15.13 g/t; Williamson and Barr 1965), and Jaccoletti South (211,400 t at 1.77 g/t; Slyth and Schwebel 1995). The total magnetic intensity image of the area (GSWA 2005) outlines a feature-less pluton with a narrow magnetic rim in meta-greywacke interpreted as massive granite (Fig. 1b). Pegmatite dikes were exposed in the Mountain Queen and adjacent mines, some steeply or shallowly dipping, and others forming structures of complex geometry. In the Comet mine, the dikes were emplaced into NW-striking reverse faults (Blatchford 1915). The pegmatites are characterized by muscovite, Mn-almandine (31 mol% spessartine), tourmaline, and rare corundum (Simpson 1952). They occur over a wide area extending past the Marvel Loch deposit (Fig. 1b).

After the completion of the northern part of the Marvel Loch open pit in 2001, declines for underground mining were developed from a portal in the central pit. The ore bodies (lodes) were extracted in 5–15 m wide stopes at an average head grade of 4.0 g/t Au until 2012, when granitic pegmatites more than 100 m thick were encountered at 650 m depth below the Boulder and East Lodes, and at about 800 m depth below the Exhibition, Sherwood and Undaunted Lodes. Diamond holes drilled from the lower mine levels intersected a large pegmatite-granite complex (Fig. 3). Zircons separated from a pegmatite dike were mostly discordant in the U-Pb system. The youngest concordant $^{207}Pb/^{206}Pb$ age (2631 ± 6 Ma) is interpreted to date emplacement, whereas ten ages of 2985 to 2646 Ma are interpreted to date xenocrysts (Wingate et al. 2012).

The Marvel Loch gold deposit

In 1995, the open pit exposed the entire mineralized SW-contact of the meta-gabbro sill (Fig. 4a), and the sub-vertical zone of magnesian tremolite-chlorite-phlogopite skarn it controls. This zone is marked by a penetrative foliation (85°-90° SW), and broadens from a width of 20 m in the northwest to 100 m at the Marvel Loch shaft, where the main branch of the sill pinches out. The boundary of the magnesian skarn with unstrained pillowed meta-komatiite maintains an orientation of N30°W / 88–90° SW throughout the open pit. A dextral-reverse sense of movement is indicated by intrafolial drag folds in diopside veins, by asymmetric biotite pressure shadows at garnets, and by arsenopyrite lineations plunging 50°-70° SE. These structures indicate that the SW-side moved up and north at the shear-zone boundary during wall-rock alteration (Mueller 1991).

Pegmatite dikes

Three thick dikes of pegmatite are exposed in the SW-wall of the Marvel Loch open pit (Fig. 4a). The northern dike terminates at the shear-zone boundary (Fig. 4b). A branch of the southeastern pegmatite is kinked down at the boundary (Fig. 4c) suggesting that the SW-side moved up during emplacement. The dikes strike north-northeast, some dip at moderate to steep angles, and others are sub-vertical (Fig. 4d). Extensions of the central and southern dikes cut across foliated magnesian skarn, where some split into meter-sized boudins. The pegmatites are banded or massive and composed of quartz, albite, microcline, muscovite, and minor biotite. Tourmaline, Mn-almandine (Fig. 4e), and Mn-apatite are accessory (1–5 vol%). The amount of microcline varies from 5 to 40 vol% in individual dikes and boudins. Boudins in magnesian skarn north of the Marvel Loch shaft lack endoskarn. Some dikes are bordered by selvages

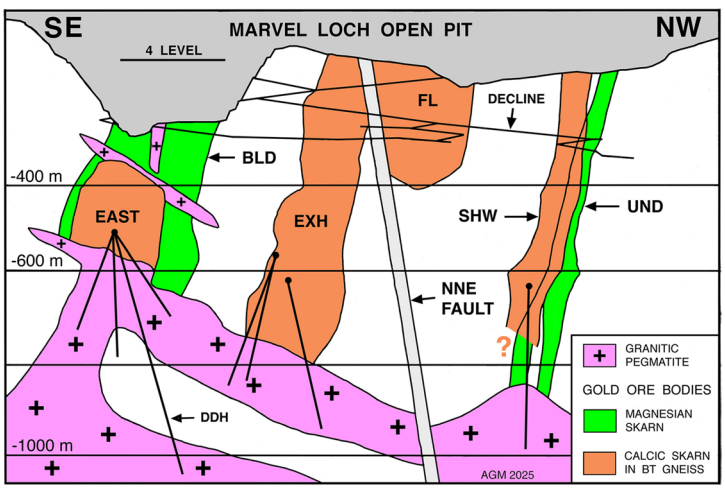

Fig. 3 Logitudinal projection of the Marvel Loch gold skarn deposit looking southwest (modified from Shenton 2013). The portal of the 2005–2012 underground mine is located in the west wall of the central open pit. The declines connecting the main ore bodies are shown on the upper levels. Each ore body was mined from ramps: the East and Boulder Lodes (BLD) down to 650 m, and the Exhibition (EXH), Firelight (FL), Sherwood (SHW) and Undaunted (UND) Lodes to 800 m below surface (= 1000 m RL). Diamond drill holes (DDH) intersected thick pegmatitic granite below all ore bodies.

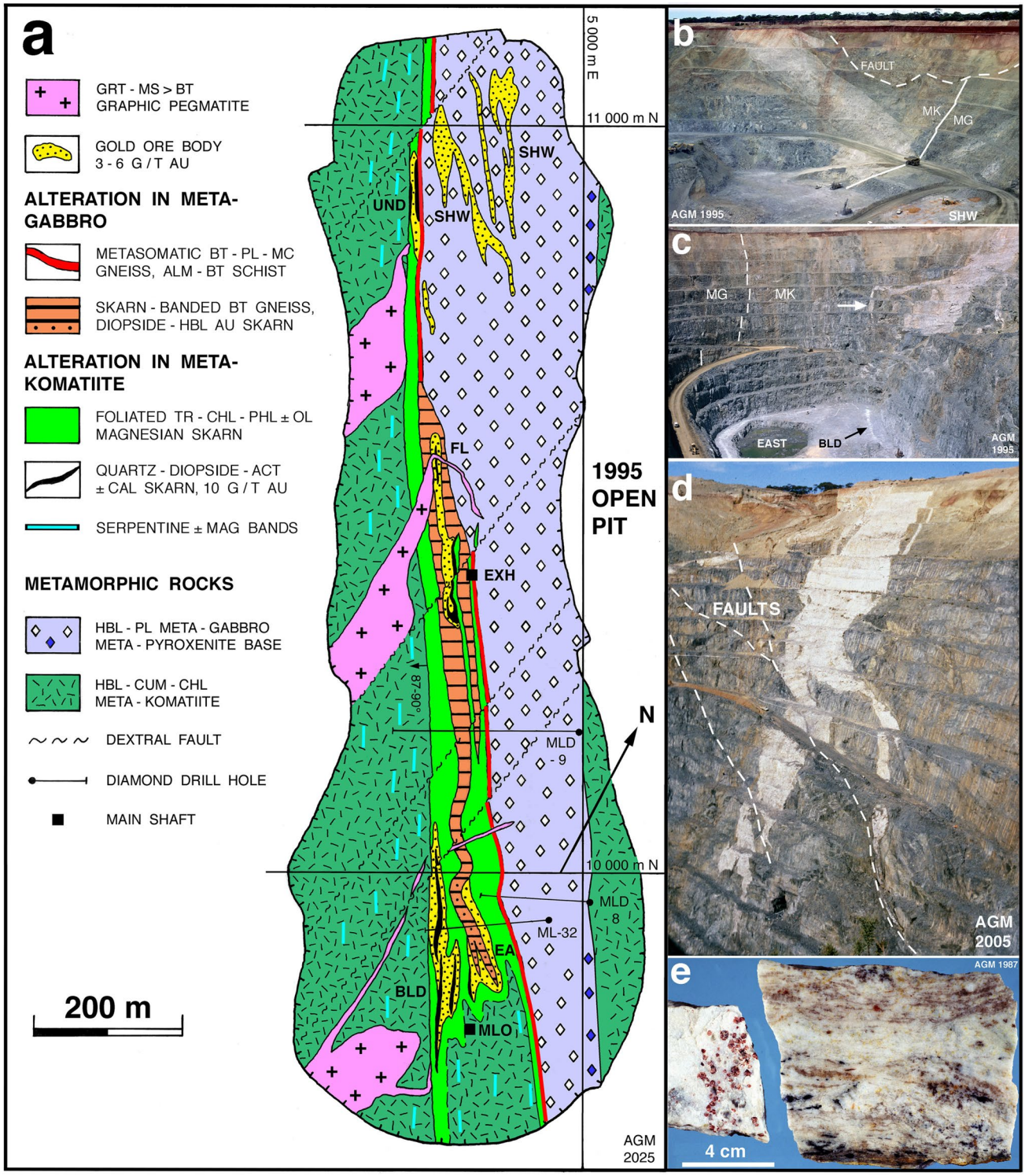

Fig. 4 Pegmatite dikes associated with the 1.5 km long alteration zone of the Marvel Loch gold skarn deposit, Southern Cross greenstone belt. **a** Geologic map of the open pit showing skarn and metasomatic gneiss bound to the contact meta-komatiite / meta-gabbro (modified from Brabham and Johnson 1995). Marvel Loch shaft (MLO). Ore bodies: Sherwood (SHW), Undaunted (UND), Firelight (FL), Exhibition (EXH), Boulder (BLD), and East Lode (EA). **b** North pit looking south in 1995, white pegmatite terminating at the altered contact meta-komatiite (MK) / meta-gabbro (MG), the Sherwood ore bodies (SHW) are in the foreground. **c** South pit looking southeast in 1995, white pegmatite in meta-komatiite, one branch kinked down (arrow) at the vertical shear-zone boundary. The excavation on the pit floor (-150 m) marks the termination of the East Lode. White blast hole dumps outline the Boulder Lode (BLD). **d** South pit looking south in 2005, NNE-striking faults offset the pegmatite dike emplaced into meta-komatiite. **e** South pit, -60 m bench, strained boudin of almandine-tourmaline-albite pegmatite in magnesian skarn

of biotite. One boudin of albite pegmatite in the open pit was partly altered to sericite + chlorite and contained native gold (Mueller 1991). A thin dike intersected by drill hole ML-4/9 contained arsenopyrite and pyrite. The mineralogical and structural features suggest that the southern pegmatite (Figs. 4c, d) was emplaced during the retrograde stage of alteration and mineralization.

Post-gold faults

An early reverse set includes shallowly west-dipping quartz-actinolite veins, flat joints and small faults in the Marvel Loch underground mine (Blatchford 1915; Mueller 1991), and one reverse fault (N45°W / 35° SW) in the Exhibition mine (Matheson and Hobson 1940). A late set comprises barren faults oriented N10°E / 75–90° W, which displace the ore bodies and the pegmatite dikes by up to 50 m in a dextral sense (Figs. 4a and d). The faults are marked by horizontal striations.

Contact alteration in meta-gabbro

Skarn-banded biotite gneiss with zones of diopside-hornblende gold skarn replaces meta-gabbro in the two sills, which branch off the main one at the Exhibition shaft and extend to the Marvel Loch workings (Figs. 4a, c). The mineralized biotite-anorthite-microcline gneiss characteristic of the East Lode, described below, pinches out NW the Exhibition (90 × 17 m, 3.5 g/t Au) and Firelight ore bodies (60 × 20 m, 2.7 g/t Au; Brabham 1995).

The SW-contact of the main meta-gabbro sill facing the East Lode-Exhibition Lode gneiss, is also altered in a 10 m wide zone marked by disseminated biotite + magnetite (Figs. 5a, b), spaced bands of biotite gneiss and almandine-biotite schist, and minor diopside-hornblende skarn. Northwest of the Firelight workings, this contact zone is 3–10 m wide and consists of biotite-plagioclase-quartz gneiss, which lacks diopside and hornblende but contains microcline (5–15 vol%), rutile (1–2%), tourmaline (0.5-2%), and pyrrhotite + pyrite (1–2%). Locally, cm-thick bands of almandine-biotite schist are intercalated. Retrograde Fe-Mg chlorite after biotite, and sericite after plagioclase are accessory.

Entirely enclosed in the main meta-gabbro sill are the 175 m long but low-grade Sherwood Lodes (Fig. 4a). The main Sherwood ore body, stoped underground at a head grade of 4.5 g/t Au over 7–8 m width and 70 m length, is located about 30 m northeast of the contact biotite gneiss. Drill hole SGC-47 intersected biotite-rich (15 vol%) gneiss containing pyrrhotite (5–10%), arsenopyrite (1–2%), and pyrite (0.5-1%). Accessory titanite (1–2%), and retrograde clinozoisite-epidote suggest that most feldspar is calcic plagioclase. Minor chlorite after biotite is widespread. The sulfide-rich ore is bordered by 1–2 m wide biotite gneiss marked by feldspar porphyroblasts and disseminated magnetite (5%). Quartz veins (2–3 vol%) contain minor feldspar + biotite, and rare actinolite + calcite.

Distal alteration in metamorphic rocks

Distal alteration in meta-gabbro and in meta-komatiite extends more then 100 m to the NE and SW of the contact-bound auriferous zone (Fig. 4a). In the meta-gabbro, such alteration comprises disseminated chlorite after hornblende, and aggregates of phengite, minor prehnite, clinozoisite and albite after calcic plagioclase (An30). In pillowed meta-komatiite (Fig. 5c), metamorphic Mg-hornblende, cummingtonite and Mg-chlorite are overprinted by widely spaced serpentine-magnetite bands (Fig. 5d) and by seams of talc-chlorite schist, distal alteration also present southeast of the Marvel Loch shaft (Fig. 4a). The pillowed units are intercalated with thin flows of peridotitic meta-komatiite, which display a metamorphic texture of randomly oriented olivine blades. Adjacent to crosscutting talc-phlogopite ± chrysotile ± pyrrhotite veins, the metamorphic olivine is replaced by lizardite ± magnetite (Fig. 5e).

Magnesian gold skarns

Most of the contact zone of magnesian skarn in meta-komatiite consists of sub-economic (0.1–0.5 g/t Au; < 1 vol% pyrrhotite) tremolite-chlorite schist with spaced seams of phlogopite (Mg_{89}; 1–10%) and porphyroblasts of olivine (Fo_{78}; 2–15%), some rimmed by lizardite + chrysotile (identified by XRD). Olivine, tremolite, and phlogopite are in part post-kinematic, and obliterate the foliation fabric locally. Primary chromite is stable but ilmenite is partly altered to rutile. Remnant domains of metamorphic hornblende-cummingtonite-chlorite rock are enclosed (Mueller 1991).

The outer tremolite-chlorite skarn contains composite bodies of olivine-calcite, diopside-actinolite, quartz-diopside, and tremolite-phlogopite skarn. These bodies are enriched in sulfides (2–5% pyrrhotite + loellingite + arsenopyrite) and form most of the low-grade ore (0.5–3 g/t Au), partly mined in the open pit but not underground. On level 4 of the Marvel Loch shaft, the distribution of the ore bodies (>1 g/t Au) has been reconstructed from the assay data of horizontal underground drill holes (Fig. 6). High-grade magnesian gold skarn (6–15 g/t Au) consists of two petrographic types, which form calcite-rich or quartz-rich tabular ore bodies sub-parallel to the foliation in the alteration zone. They are represented by the Savage and Boulder Lodes, respectively. Both retain the high-Mg, high-Cr, high-Ni and low-Zr signature of the meta-komatiite and the outer skarn they progressively replace (Table 1).

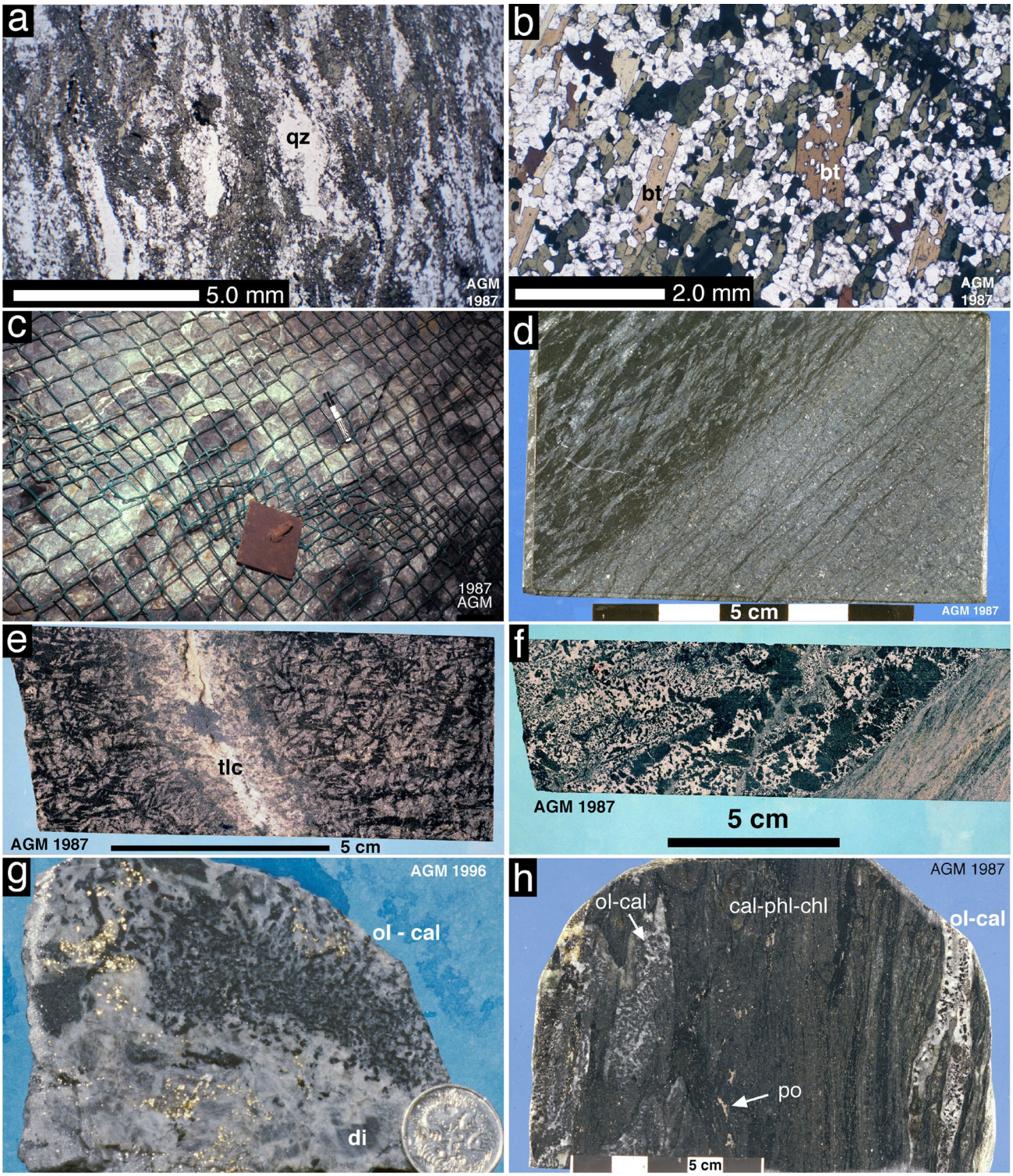

Fig. 5 Photographs of metamorphic rocks, distal wall-rock alteration, and calcite-rich magnesian skarn, Marvel Loch (a-f, h) and Yilgarn Star (g) gold deposits, Southern Cross Belt. **a** Meta-gabbro: hornblende + plagioclase (An30) ± quartz (qz) ± ilmenite, drill hole ML-4/8, 96.0 m, plane polarized light. **b** Biotite (bt) + magnetite (opaque) alteration in meta-gabbro, drill hole ML-4/9, 50.1 m, PPL. **c** Pillowed meta-komatiite (21 wt% MgO): hornblende + cummingtonite + chlorite, 25 m grid east of the Marvel Loch shaft on 4 level, the pen is 14 cm. **d** Black lizardite ± magnetite alteration in meta-komatiite, drill hole MLD-9, 305.6 m. **e** Peridotitic meta-komatiite (37% MgO): lizardite after bladed metamorphic olivine, vein of talc (tlc) + phlogopite ± pyrrhotite, drill hole EXHD-23 A, 157.5 m. **f** Olivine-calcite skarn, serpentine + magnetite after olivine, retrograde talc, drill hole MLD-9, 298.8 m. **g** Yilgarn Star South Lode: native gold in olivine-calcite (ol-cal) + diopside (di) skarn, stope at 2220–2260 m RL, the coin is 19 mm. **h** Savage Lode: olivine-calcite skarn (ol-cal) in calcite-phlogopite-chlorite (cal-phl-chl) schist, disseminated pyrrhotite (po) + loellingite, Marvel Loch shaft 4 level

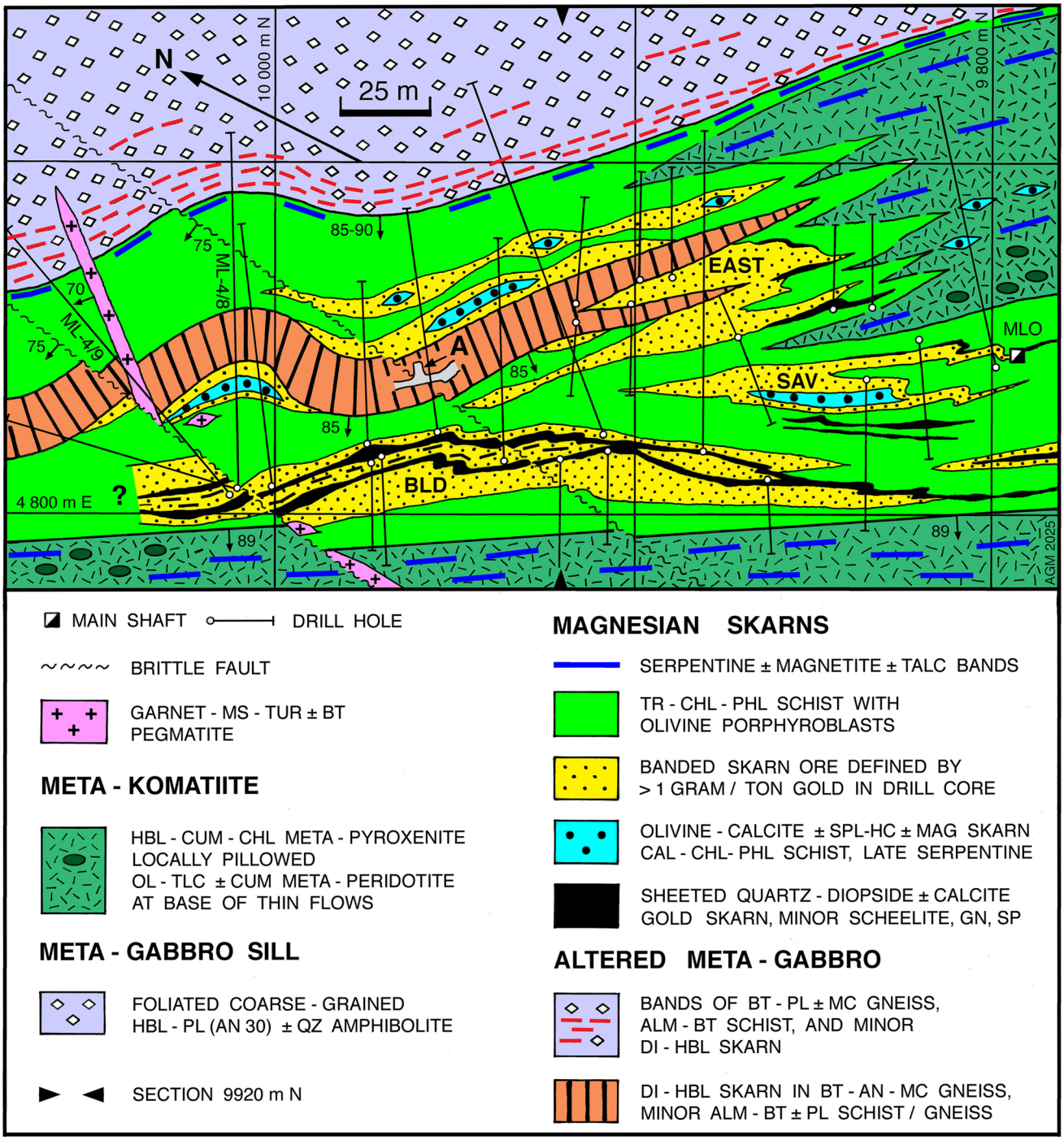

Fig. 6 Geologic map of the Marvel Loch shaft (MLO) 4 level showing the SE-part of the skarn zone at the contact meta-komatiite / meta-gabbro based on the level plan in Mueller (1991) and cross sections in Brabham (1995). Low-grade ore (> 1 g/t Au) is contoured from the intersections of flat drill holes on levels 3 and 4 (92 and 122 m below shaft collar). Ore bodies (4–10 g/t Au) are the Boulder (BLD) and Savage Lode (SAV) magnesian skarns in meta-komatiite, and the East Lode (EAST) skarn-banded gneiss in meta-gabbro. Note the position (A) of the East Lode petrographic section (Fig. 9). Almandine (alm), anorthite (an), biotite (bt), calcite (cal), chlorite (chl), cummingtonite (cum), diopside (di), galena (gn), hercynite (hc), hornblende (hbl), magnetite (mag), microcline (mc), muscovite (ms), olivine (ol), phlogopite (phl), plagioclase (pl), quartz (qz), sphalerite (sp), spinel (spl), talc (tlc), tourmaline (tur), tremolite (tr)

Savage Lode gold skarn

Gold skarn rich in calcite (6–8 mol% $MgCO_3$; 30–40 vol%) formed the main part of the Savage Lode (6.4 g/t Au) on level 4 of the Marvel Loch shaft, an ore body 4–5 m wide and 30 m long. Calcite-rich skarn does not always constitute ore, for example at the contact of the main meta-gabbro sill, where retrograde serpentine + magnetite overprint olivine-calcite assemblages (Fig. 5f). In contrast, spectacular grade (97 g/t Au) has been reported from the Yilgarn Star deposit SE of Marvel Loch (Fig. 1a), where olivine-calcite-diopside skarn mineralized with native gold (Fig. 5g) is typical of the southern ore body (90 × 20 m, 370 m down-plunge; Witt et al. 2001).

The core of the Savage Lode is composed of calcite-phlogopite-chlorite schist enclosing lenses of olivine-calcite (Fig. 5h), diopside ($Di_{88–91}$), and tremolite-actinolite skarn. Minor dolomite (1–5%) and scheelite (1–2%) are disseminated. The calcite-rich ore is bordered by sulfide-rich but calcite-poor gold skarn, where abundant diopside ($Di_{71–93}$) is intercalated with Mg-hornblende bands, tremolite-actinolite lenses, and quartz-diopside veins (Fig. 7 in Mueller 1991).

The olivine-calcite skarn in the Savage Lode contains clusters of native gold, interstitial Mg-chlorite, and disseminated green spinel, which forms aggregates with subhedral Mg-Mn ilmenite (<1 mol% Fe_2O_3). The green spinel is a spinel-hercynite solid solution (X_{spl} 0.52, X_{hc} 0.34) with negligible magnesioferrite (X_{mfr} 0.02), magnetite (X_{mag} 0.01), and other

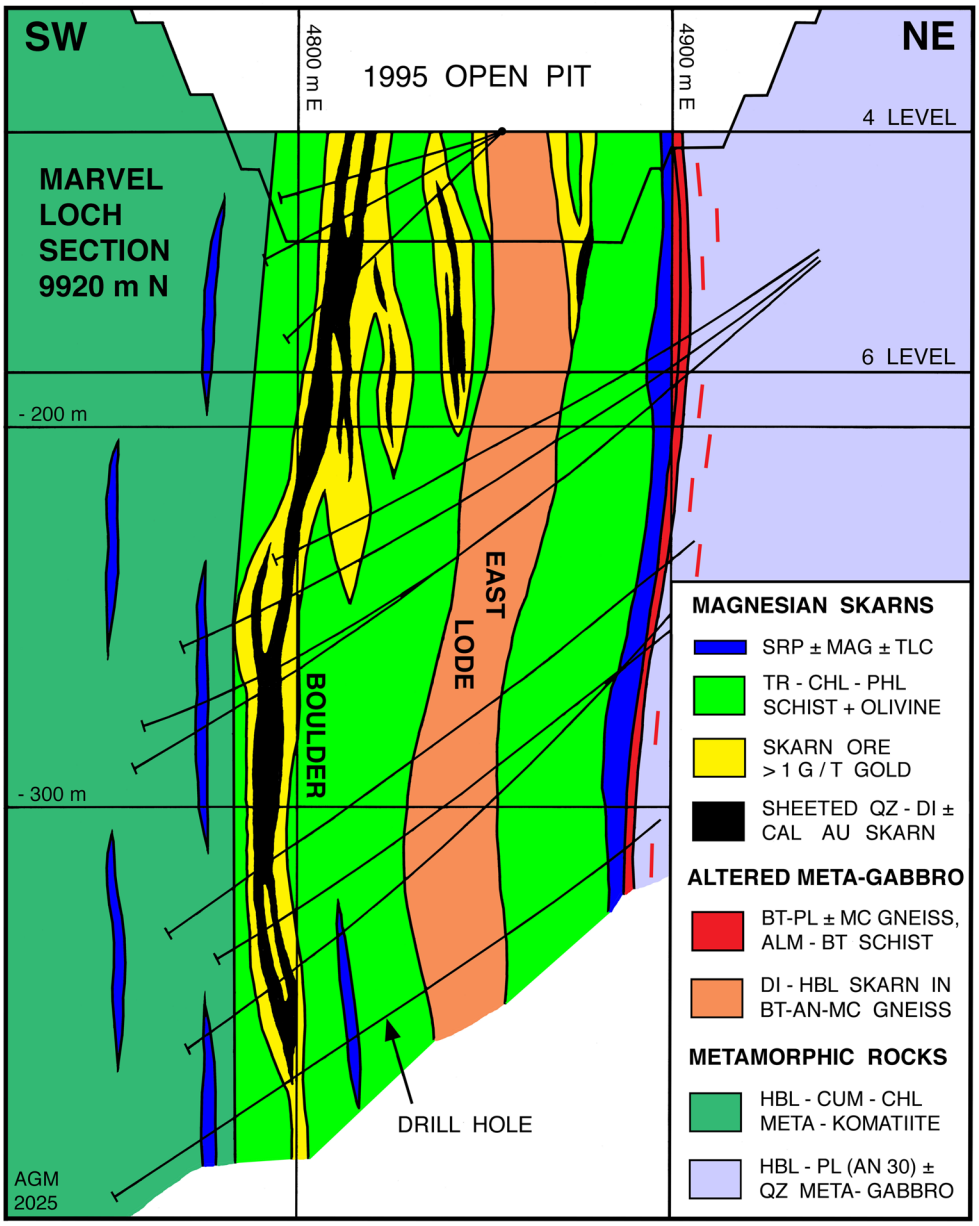

Fig. 7 NE-SW section through the Marvel Loch skarn zone enclosing the Boulder Lode and East Lode ore bodies at mine grid 9920 m N (modified from Brabham 1995). The geology is projected up to the 4 level of the Marvel Loch shaft above the March 1995 pit floor

components (ESM Table 5). Magnetite (3 vol%) rims and partly replaces the spinel-ilmenite aggregates, and forms thin layers in the {001} cleavage of Mg-chlorite. The magnetite (X_{mag} 0.90, X_{mfr} 0.03, X_{chr} 0.03) contains no ulvöspinel (ESM Table 5), and is particularly abundant in intermediate-stage calcite-chlorite-phlogopite schist. Consequently, the Fe^{3+}/Fe_{total} ratio (0.201) of the calcite-rich ore is more than 6-times higher than the ratio of diopside skarn at its margin, which is equivalent to that of the meta-komatiite host rock (0.030; Mueller et al. 1991).

Disseminated pyrrhotite and loellingite (2–5 vol%) replace both magnetite and silicates including post-kinematic chlorite and phlogopite in the intermediate-stage schist. Pyrrhotite is intergrown with chalcopyrite (0.1%) and very rare pyrite, whereas loellingite is rimmed by niccolite (0.3%) and by accessory arsenopyrite. Retrograde silicates are minor (<5 vol%) and mostly free of sulfides. Some olivine grains are rimmed by serpentine, and rare talc replaces diopside or tremolite. In diopside-rich skarn, muscovite+zoisite/clinozoisite±prehnite replace interstitial aggregates (1–2 vol%) of calcic plagioclase±microcline (Mueller 1991).

Boulder Lode gold skarn

Skarn composed of quartz (50–70 vol%), diopside (Di_{88-94}; 10–30%), tremolite-actinolite (5–20%), phlogopite (5–10%), calcite (5%) and scheelite (0.5-1%) constituted the Boulder Lode, at 240 m length and 8–10 m width the largest ore body at Marvel Loch (Figs. 6 and 7). The southern (70 m) and northern sections (85 m) averaged 6.5 g/t Au while the central section was lower in grade (3.6 g/t; Brabham 1995). Shorter quartz-diopside ore bodies (<80 m) were part of the Exhibition Lode (5–10 g/t Au) and formed the Undaunted Lode (14–18 g/t Au) in the central and northern parts of the open pit (Fig. 4a). On the upper mine levels, the Boulder Lode contained more diopside (average 30%) than actinolite (5–10%) in comparison to the Undaunted Lode, where actinolite (20%) was dominant over diopside (10%). The ore bodies are composed of sheeted quartz-diopside-actinolite veins (Fig. 8a), and of quartz-rich replacement in tremolite-phlogopite-chlorite schist (Fig. 8b). Some veins have a pinch-and-swell structure, many are banded, and others are massive. The 1986 mill-head sample (1735 t) of Boulder Lode sulfide ore contains 9.93 g/t Au. The Fe^{3+}/Fe_{total} ratio (0.093) is higher than that of the ultramafic host rock (0.030).

Silver-rich gold (0.1–5 mm) occurs enclosed in quartz and diopside, and is associated with scheelite, hexagonal pyrrhotite (Fig. 8c), minor arsenopyrite, pyrite, and aggregates (0.5-1 vol%) of galena, iron-rich sphalerite with chalcopyrite blebs, chalcopyrite, and tennantite. Native bismuth is enclosed in quartz and in sulfide aggregates (Fig. 8d), and is in contact with silver-rich gold (Figs. 8e and f). Some of the native bismuth is rimmed by thin seams of pure gold (Fig. 8e).

East Lode gold skarn and gneiss

The East Lode consists of diopside-hornblende gold skarn in biotite-anorthite-microcline gneiss and of almandine-biotite schist, which replace meta-gabbro in the SW-branch of the main sill terminating at the Marvel Loch shaft (Fig. 4a). This structure controls the 75 m long and up to 25 m wide East Lode ore body composed of calcic skarn in gneiss and of magnesian contact skarn (Fig. 4c). The composite SE-part of the East Lode averaged 3.7 g/t Au but the ore extends another 130 m northwest, where it narrows to 10 m at 2.2 g/t Au (Brabham 1995). The East Lode retains the low-Mg, high-Ti and high-Zr signature of the precursor meta-gabbro (Table 1).

Zoned alteration in the East Lode

The East Lode on the Marvel Loch shaft 4 level was developed via a central drive connected to crosscuts for upward stoping (Fig. 2 in Mueller 1991). The alteration zone in one crosscut (location A in Fig. 6) was mapped at a scale of 1:25 (Fig. 9), and sampled for geochemical analysis (ESM Table 1). The petrographic units include partly altered meta-gabbro and barren garnet-biotite schist and garnet gneiss in the northeast, and sulfide-rich calcic gold skarn and skarn-banded gneiss in the southwest. Primary sulfides were preserved except for thin rims and veinlets of supergene pyrite and marcasite (<0.5 vol%) in pyrrhotite.

Altered meta-gabbro This outer unit differs from least-altered meta-gabbro by higher CaO/Na_2O and K_2O/Na_2O ratios, by higher As and Ba, and by 0.41 g/t Au (ESM Table 1). It is crosscut by thin quartz-diopside veins (Fig. 9), and composed of remnant meta-gabbro overprinted by metasomatic hornblende, calcic plagioclase (An90?), quartz, biotite, and accessory microcline and calcite. On average, the mineral composition is Fe-Mg hornblende (40 vol%), plagioclase (30%), quartz (15%), biotite (10%), and microcline (3%). Epidote (2%), titanite (0.5%), and ilmenite-rutile aggregates (0.5%) are accessory. Magnetite is absent. Retrograde alteration (5–7%) led to the partial replacement of hornblende by epidote+titanite, of calcic plagioclase by phengite+clinozoisite, and of biotite by Fe-Mg chlorite. Late-stage sulfides (1–2%) include arsenopyrite, minor pyrrhotite, pyrite, and trace chalcopyrite.

Almandine-biotite schist This unit represents early-stage alteration, as it is crosscut by laminated quartz-diopside-anorthite skarn (Fig. 10a), the calcic plagioclase partly replaced by phengite+clinozoisite. A quartz-arsenopyrite vein cuts across the laminated skarn in turn (Fig. 9) indicating successive replacement stages and late sulfide

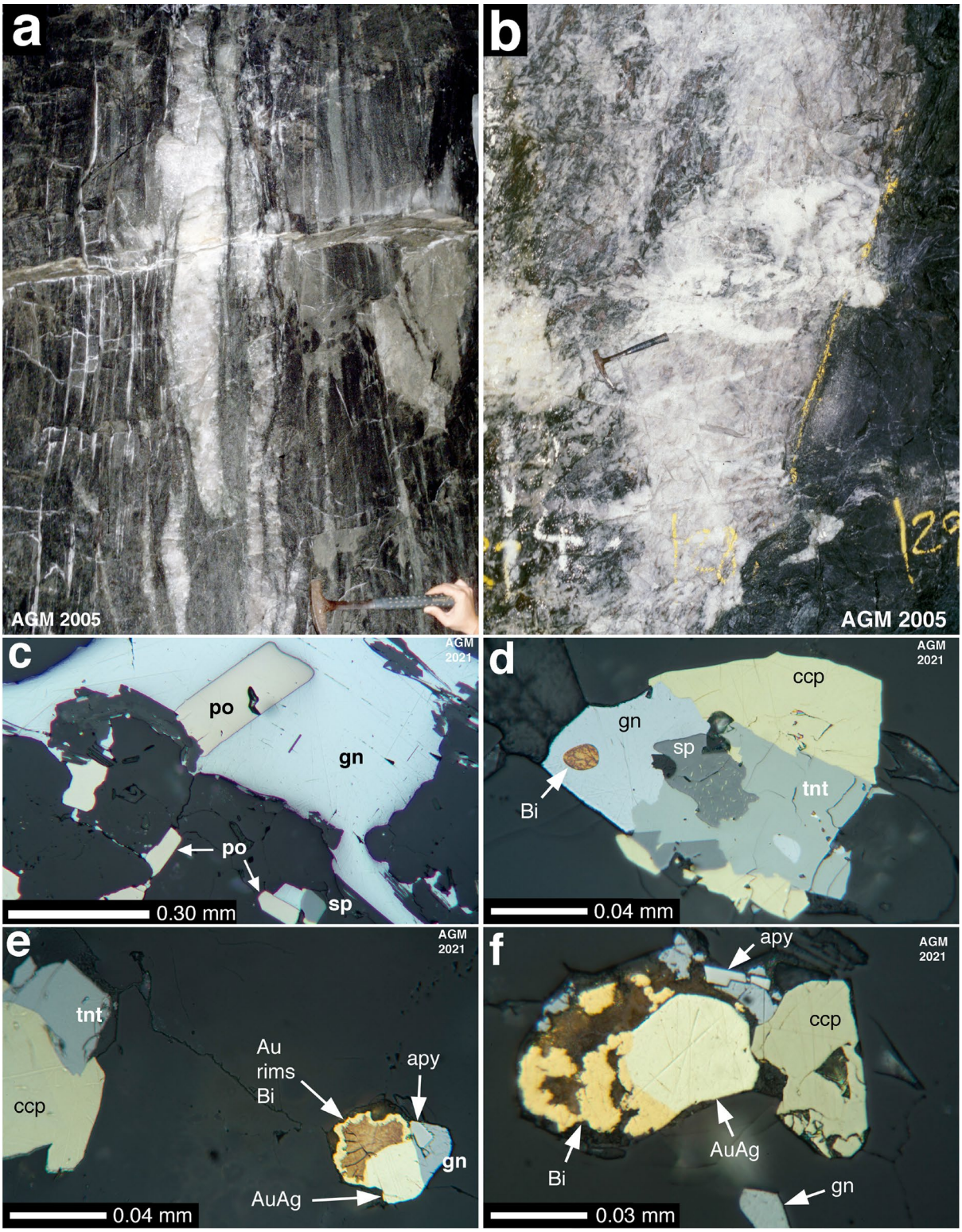

Fig. 8 Photographs of quartz-diopside-actinolite skarn of the Undaunted Lode, Marvel Loch deposit. **(a)** Undaunted Lode at 755 m RL looking NW at sheeted quartz-di-act veins in actinolite-chlorite ± phlogopite schist.The hammer is 32 cm. **(b)** Undaunted Lode at 675 m RL looking west at quartz-di-act replacement in actinolite-phlogopite-chlorite schist. **(c)** Hexagonal pyrrhotite (po) in galena (gn), minor sphalerite (sp), plane polarized light reflected in air. **(d)** Native bismuth (Bi) in galena (gn), sphalerite (sp), tennantite (tnt) and chalcopyrite (ccp). PPL in air. **(e)**Native bismuth (Bi) rimmed by pure gold (Au), silver-rich gold (AuAg), arsenopyrite (apy) and galena (gn) adjacent to chalcopyrite (ccp) + tennantite (tnt). PPL in air. **(f)** Native bismuth (Bi) and silver-rich gold (AuAg), galena (gn), arsenopyrite (apy), and chalcopyrite (ccp). PPL in air

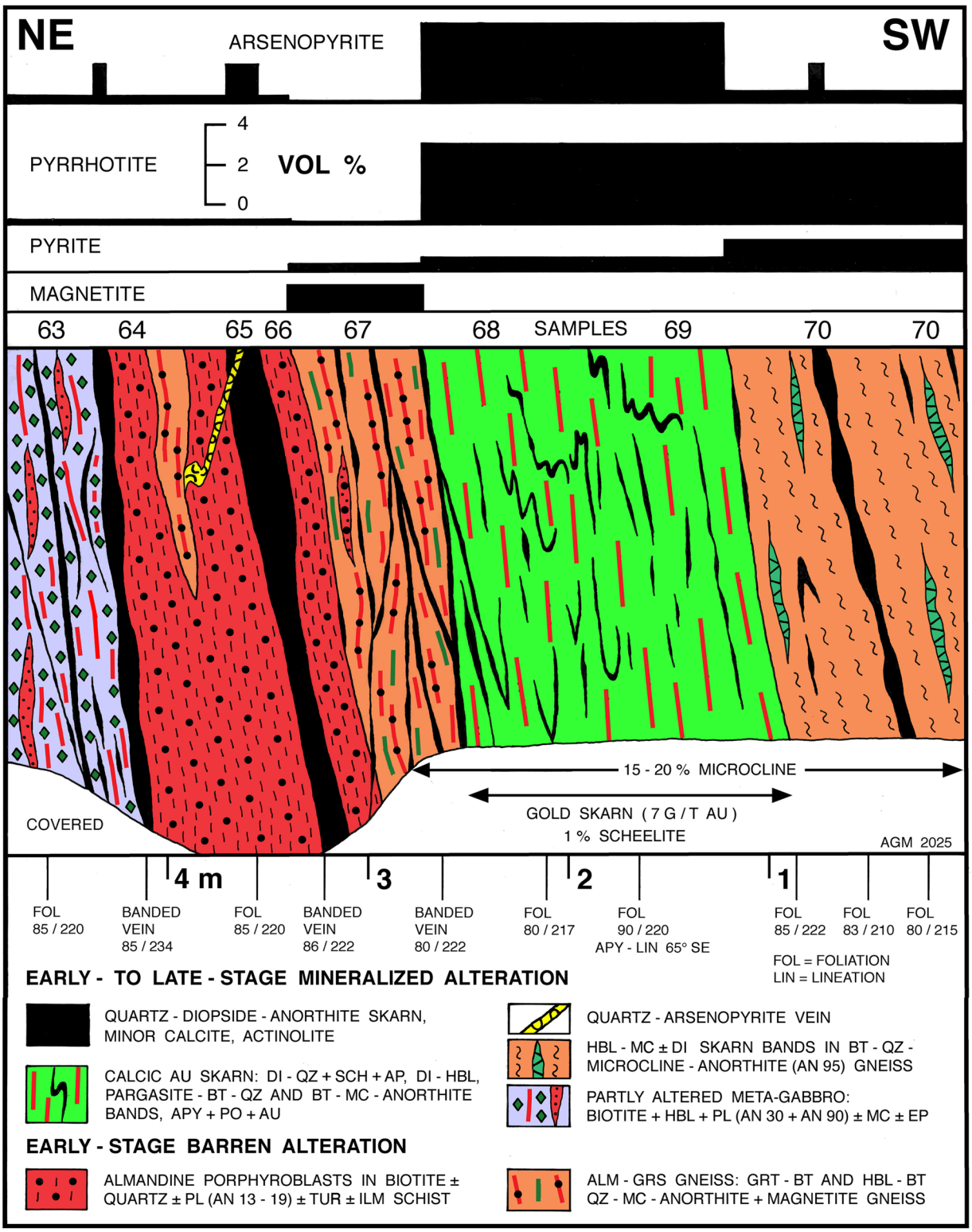

Fig. 9 Looking southeast at a cross section through zoned East Lode replacement in meta-gabbro: almandine-biotite schist, almandine-grossular gneiss, diopside-hornblende gold skarn, and skarn-banded biotite-anorthite-microcline gneiss. Marvel Loch shaft 4 level at mine grid 9960 m N (location A in Fig. 6). The structural data are in dip + dip direction. The calc-silicate anorthite has been identified by XRD (ESM page 6–7), by EPMA (ESM Table 2d), and indirectly by whole-rock analysis (ESM Table 1)

deposition. The almandine-biotite schist is enriched in titanium, and in both ferric (4.22 wt%) and ferrous iron oxide (19.26%; Fe3+/Fe_{total} = 0.165) relative to least-altered metagabbro. Sulfur (0.05%) and gold (18 ppb) are low but arsenic and tungsten are enriched (Table 1). The schist consists of porphyroblasts and aggregates (25–30 vol%) of almandine ($Alm_{88–90}$ Sps_2 Grs-$Adr_{2–5}$) in equilibrium contact with Fe-biotite ($Mg_{17–23}$; 40 vol%) and tourmaline (Fig. 10b). Biotite, plagioclase, quartz, ilmenite and staurolite (Fig. 10c) are enclosed in garnet cores. Fe-rich chlorite (Mg_{23}; 2%) is in contact with garnet, lines cracks in garnet, and is interlayered with biotite. Quartz (10–15%), oligoclase (An13-19), and ilmenite (2%) are interstitial. Microcline and carbonate are absent.

Almandine-grossular gneiss Garnet-bearing biotite gneiss, crosscut by thin (1–5 cm) quartz-diopside veins, forms a transitional unit between the early-stage almandine-biotite schist and calcic gold skarn (Figs. 9 and 10a). Bands of microcline (10 vol%) result in a K_2O/Na_2O ratio higher than in almandine-biotite schist (ESM Table 1). The sulfur, arsenic, and gold contents of the whole rock are low. The gneiss consists of fine-grained biotite (15–20%), hornblende (5–10%), anorthite (An90), and quartz (10–15%). It is characterized by aggregates (5–10 vol%) of almandine-grossular garnet ($Alm_{63–65}$ $Sps_{5–7}$ $Grs_{22–26}$ $Adr_{3–4}$), by tourmaline (0.5-3%), and by evenly disseminated magnetite (1–2%). Ilmenite and rutile are accessory. The magnetite is associated with late-stage pyrite (0.5%), and with trace chalcopyrite and pyrrhotite (Fig. 10d). Garnet and biotite are replaced by minor Fe-chlorite, and anorthite is partly retrograded to phengite, clinozoisite, calcite, and rare prehnite.

Diopside-hornblende gold skarn The calcic skarn on 4 level is 1.5 m thick and contains 7 g/t gold (Fig. 9). Sulfur, arsenic and tungsten reach percent concentrations (Table 1). The skarn is characterized by numerous intrafolial quartz-diopside-hornblende veins. The vein quartz (20–50%) is intergrown with minor calcite, calcic plagioclase, and biotite. Many veins and bands of diopside ($Di_{56–70}$) + quartz (Fig. 10e) are zoned to outer Mg-hornblende and/or potassian ferro-pargasite (ESM Table 2c). The calc-silicates are in contact with aggregates of Mg-chlorite (Fig. 10f), titanite ± rutile, and with interstitial anorthite (An90) partly replaced by retrograde phengite, clinozoisite, calcite, and albite. Intercalated bands consist of biotite (20%), quartz, microcline, and anorthite. The calcic-potassic nature of the skarn is reflected in high CaO/Na_2O and K_2O/Na_2O ratios (ESM Table 1). Blue-fluorescent scheelite and apatite are most abundant in veins (Fig. 10g). The assemblage of late-stage sulfides (8–15 vol%) comprises arsenopyrite, pyrrhotite, minor chalcopyrite, and silver-rich native gold (Fig. 10h). Accessory pyrite and trace marcasite are in contact with arsenopyrite and pyrrhotite.

Skarn-banded biotite gneiss Biotite-anorthite-microcline gneiss (Fig. 11a) is >22 m thick on 6 level, and represents the main alteration facies on 4 level. The abundance of anorthite and microcline is reflected in the high CaO/Na_2O and K_2O/Na_2O ratios of the total rock (ESM Table 1), and the abundance of sulfides in high sulfur contents (3.7–4.4 wt%). The average gold grade is low (0.3–0.4 g/t). The gneiss consists of fine-grained biotite (10–20 vol%), anorthite (An94-96; ESM Table 2d), locally in 5–10 mm porphyroblasts (Fig. 11b), quartz (20%), microcline (10–20%), pyrrhotite and pyrite (7–10%), accessory rutile + titanite (1–2%), and widely spaced seams of bright green fuchsite (1%). Locally, microcline replaces anorthite at grain boundaries and along cleavage planes. Retrograde minerals (5–10 vol%) are concentrated in spaced bands, where the anorthite is selectively replaced by aggregates of clinozoisite, prehnite, and phengite (Fig. 11c). Adjacent biotite is altered to Fe-Mg chlorite and encloses lenses of prehnite parallel to its {001} cleavage (ESM Table 2d).

Apart from anorthite, prograde skarn bands consist of Mg-hornblende intergrown with microcline and minor quartz. Blebs of pyrrhotite and minor pyrite are enclosed in the silicates (Fig. 11d). Many hornblende blades (5–20 mm), locally associated with diopside (1–2%), are oriented at a high angle to the biotite foliation (Fig. 11e). Scheelite-bearing quartz-diopside veins up to 20 cm thick, some folded and others with pinch-and-swell structure, are widely spaced. The diopside ($Di_{83–87}$) is more magnesian than in the main calcic gold skarn, intergrown with quartz and minor calcite, and zoned to outer actinolite. The veins are selectively mineralized with arsenopyrite, pyrrhotite, minor galena, pyrite, and rare marcasite (Fig. 11f), and increase the gold grade of the gneiss.

Sulfide assemblages

The sulfide assemblages of the gold skarns described above differ in mineralogy and abundance. Scheelite is present in all ore bodies but reaches by-product grade only in small volumes of skarn. The ore minerals of the Savage, Boulder and East Lodes are linked to the respective gangue in Fig. 12, which provides a paragenetic overview for the discussion of PTX-constraints. The Savage Lode magnesian skarn is low in sulfur (1.04 wt% S; Table 1), and the sulfide assemblage is dominated by disseminated

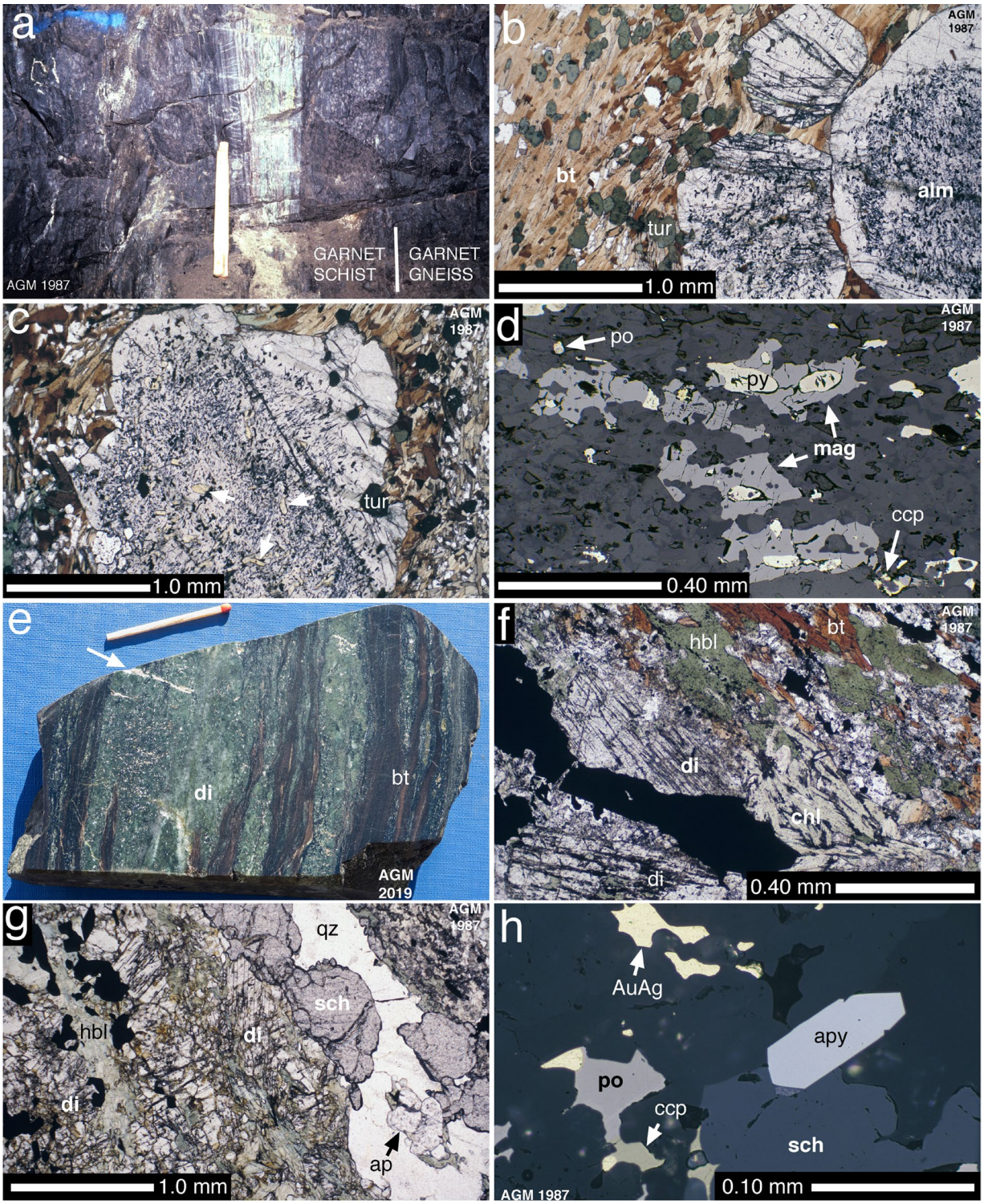

Fig. 10 Photographs of East Lode almandine-biotite schist, almandine-grossular gneiss, and diopside-hornblende gold skarn (see Fig. 9), Marvel Loch shaft 4 level. **a** Qz-di-an skarn crosscuts alm-bt schist grading into alm-grs gneiss, looking SE, the scale is 21 cm. **b** Alm-bt schist: Almandine (alm) in contact with biotite (bt) and tourmaline (tur), interstitial quartz and oligoclase, plane polarized light. **c** Alm-bt schist: Almandine with inclusions of staurolite (arrows), biotite, opaque ilmenite, and tourmaline (tur), PPL. **d** Alm-grs gneiss: Early magnetite (mag), late pyrite (py), pyrrhotite (po) and chalcopyrite (ccp), PPL reflected in air. **e** Diopside (di) ± quartz skarn zoned to hornblende + biotite (bt), 10% arsenopyrite + pyrrhotite ± gold, tension-gash sulfide veins (arrow), the matchstick is 42 mm. **f** Calcic skarn: Diopside (di), hornblende (hbl), biotite (bt) and Mg-chlorite (chl) replaced by opaque sulfides, PPL. **g** Calcic skarn: Diopside (di), hornblende (hbl), and sulfides border a vein of quartz (qz), scheelite (sch), and apatite (ap), PPL. **h** Calcic skarn: Scheelite (sch), arsenopyrite (apy), pyrrhotite (po), chalcopyrite (ccp), and silver-rich gold (AuAg), PPL reflected in air

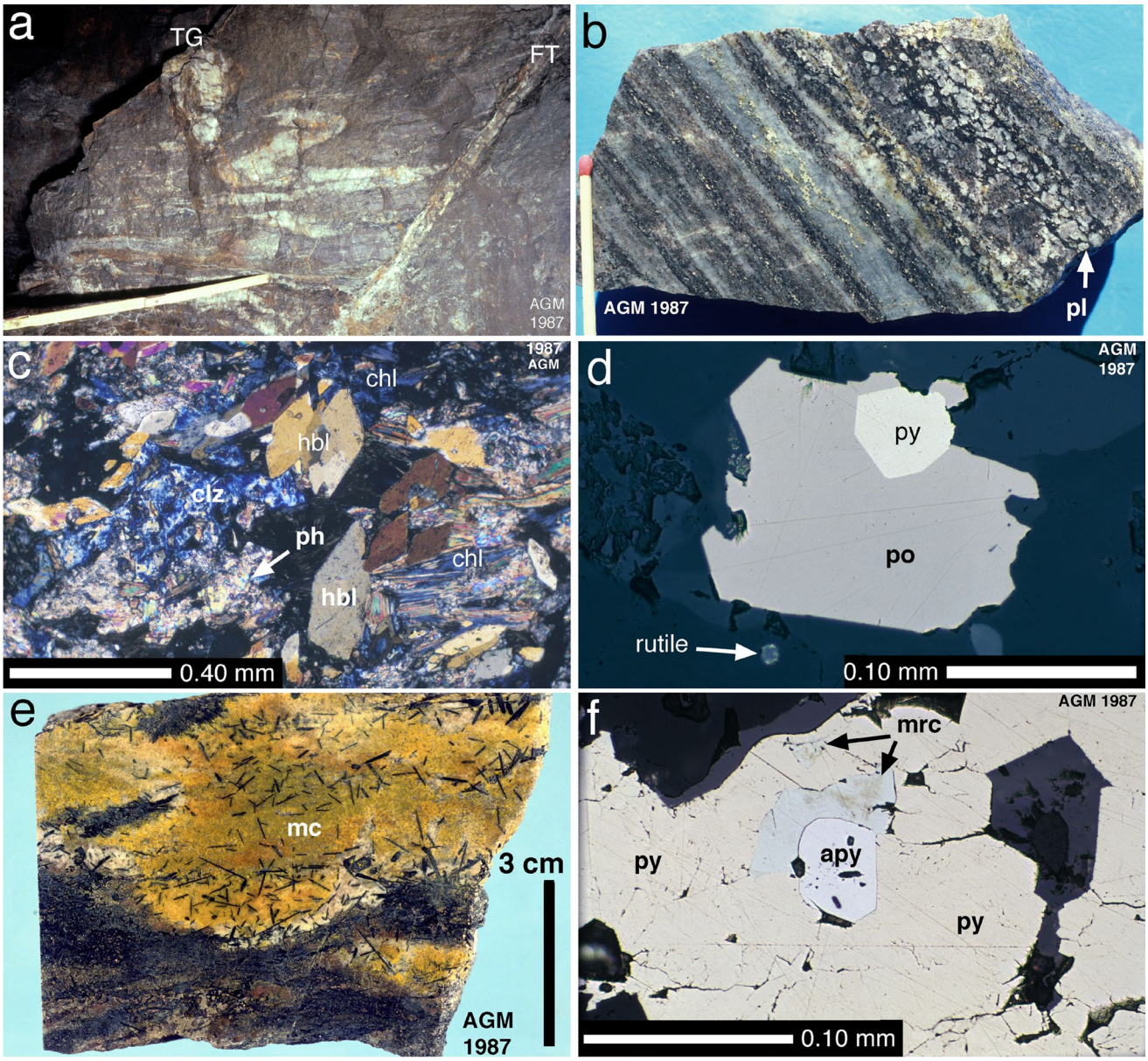

Fig. 11 Photographs of skarn-banded biotite-anorthite-microcline gneiss, East Lode, Marvel Loch shaft 4 level (9960 m N) and 6 level (9870 m N). **a** Folded quartz-diopside and tension-gash (TG) veins in gneiss are offset at a NNE-striking fault (FT), 4 level, looking up, the scale is 42 cm. **b** Gneiss on 6 level, anorthite porphyroblasts (pl), 5–7% pyrite + pyrrhotite, the matchstick is 3.5 cm. **c** Gneiss on 4 level: Prograde hornblende (hbl), retrograde chlorite (chl) after biotite, and clinozoisite (clz) + phengite (ph) after anorthite, crossed polars. **d** Gneiss on 4 level: Subhedral pyrite (py) rimmed by pyrrhotite (po), plane polarized light reflected in air. **e** Gneiss on 6 level: Black hornblende in microcline (mc, stained yellow), minor quartz, titanite, and pyrrhotite (5 vol%). **f** Quartz-diopside skarn in gneiss on 4 level: Arsenopyrite (apy) and marcasite (mrc) enclosed in pyrite (py), PPL reflected in air

pyrrhotite and Ni-rich loellingite. Olivine-calcite skarn contains silver-poor native gold (5 at% Ag; ESM Table 4) but the Au/Ag ratio of the ore body (Au/Ag = 1.28) suggests the presence of electrum (?), possibly attached to arsenides in calcite-chlorite-phlogopite schist.

The Boulder Lode quartz-diopside skarn is also low in sulfur (0.62 wt% S) and has a higher Au/Ag ratio (1.74) than the Savage Lode despite the presence of silver-rich gold (22 at% Ag; ESM Table 4). Loellingite is absent but hexagonal pyrrhotite and arsenopyrite are common. Base-metal sulfide aggregates (galena, Fe-sphalerite, chalcopyrite), tennantite, silver-rich gold and, locally, native bismuth alloyed with pure gold are characteristic.

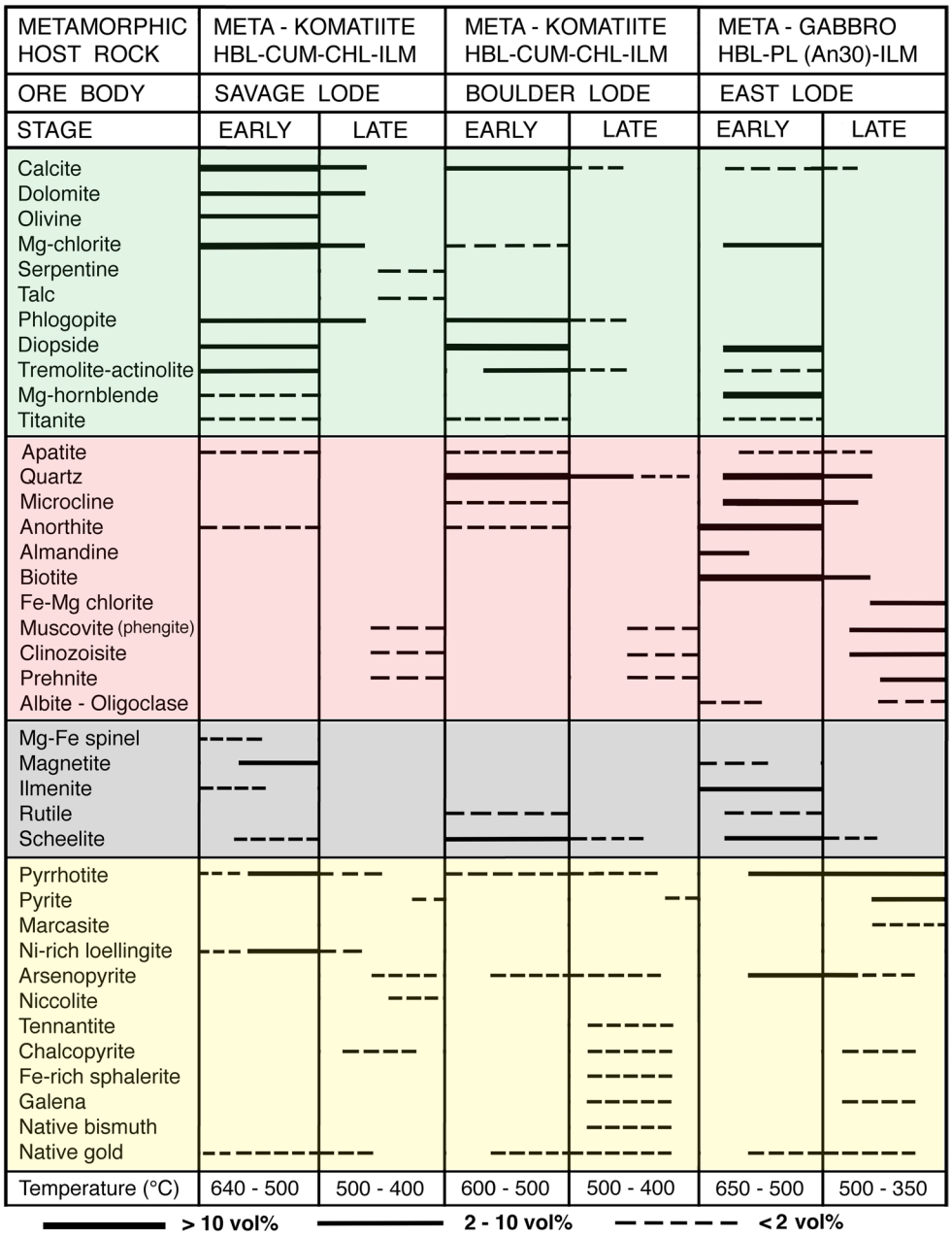

Fig. 12 Paragenetic diagram for the Savage Lode, Boulder Lode and East Lode gold skarns linking gangue to sulfide mineralogy according to temperature constraints imposed by early and late assemblages in the ore bodies. Calcite-rich cal-ol-chl-spl-ilm and cal-phl-chl-mag gold skarn is restricted to the Savage Lode, whereas quartz-rich di-act-cal skarn forms the Boulder Lode and veins in all units of the East Lode

Both the East Lode diopside-hornblende gold skarn (4.20 wt% S) and the low-grade skarn-banded gneiss (4.38 wt% S) are much higher in sulfur content than the magnesian ore bodies. The Au/Ag ratio varies widely from 9.7 in the skarn to 0.52 in the gneiss (Table 1). The diopside zones and bands in the East Lode gneiss also vary in quartz abundance, and locally approach the magnesian and quartz-rich nature of the Boulder Lode. The sulfide assemblage is similar, too: arsenopyrite and pyrrhotite, minor chalcopyrite, galena, and silver-rich gold (22–23 at% Ag; ESM Table 4) are present but tennantite and native bismuth have not been detected. Arsenopyrite is largely absent in the biotite-anorthite-microcline gneiss (427 ppm As; Table 1), where the assemblage pyrrhotite + pyrite predominates. Accessory marcasite is characteristic of the East Lode sulfide ore.

Constraints on metasomatism

Mass balance calculations after the isocon method of Grant (1986) using the data in Table 1 were carried out to constrain the nature of metasomatism in the Savage and Boulder Lode magnesian gold skarns, in the East Lode diopside-hornblende gold skarn, and in the East Lode biotite-anorthite-microcline gneiss and almandine-biotite schist (ESM Fig. 1).

Least-mobile elements

In hydrothermal systems, Al, Ti and Zr are generally regarded as least-mobile elements (Grant 1986; Côté-Mantha et al. 2012). In the calcite-rich gold skarn of the Savage Lode, Al and the total rare earth elements (REE) are least mobile relative to concentrations in meta-komatiite but MgO, Zr (in zircon), and Cr (in chromite) also plot on or close to the Al-REE isocon. In the bulk quartz-diopside ore from the Boulder Lode, the Cr-Zr isocon shares its least-mobility status with Ti, Al and MgO. A moderate volume increase is indicated due to the deposition of calcite- or quartz-rich veins in foliation planes.

In the three East Lode samples, Ti (in ilmenite-rutile) and Zr (in zircon) are least mobile relative to concentrations in the meta-gabbro host rock. The isocons indicate equal-mass replacement for both the diopside-hornblende gold skarn and the biotite-anorthite-microcline gneiss. In contrast, the Ti-Zr isocon indicates a volume decrease for the early-stage almandine-biotite schist.

The total REE plot on or close to the lithophile element isocons of all samples (ESM Fig. 1) permitting an independent check on provenance and on volume change. The chondrite-normalized patterns of the five altered rocks are parallel to those of the host rocks (ESM Fig. 2) confirming inheritance and insignificant changes in REE-mass. In the case of both magnesian gold skarns, the patterns plot below that of the pillowed meta-komatiite consistent with a volume increase of about 30 per cent. The pattern of the almandine-biotite schist plots above that of the meta-gabbro indicating a decrease.

Mobile major elements

Metasomatic element mobility relative to the host rock (±30% or 3x the accuracy) in the Savage, Boulder and East Lode gold skarns (ESM Figs. 1a-c) is distinct from that in low-grade biotite gneiss and in almandine-biotite schist (ESM Figs. 1d, e). In the Savage Lode, CaO, CO_2, K_2O, Fe_2O_3 and S are strongly enriched. The same enrichment pattern is evident in quartz-diopside skarn from the Boulder Lode, and in calcic gold skarn from the East Lode. In the latter, the pattern is subdued due to the per cent concentrations of W and As (Table 1). The selective enrichment in P_2O_5 (ESM Fig. 1c) in the calcic gold skarn is caused by apatite in veins. The low-grade biotite gneiss of the East Lode is enriched in S and K_2O, and the barren almandine-biotite schist in K_2O. Na_2O is consistently depleted in all altered rocks, whereas Fe_2O_3 is enriched in those analyzed by Mössbauer spectroscopy (Table 1).

Litho- and chalcophile trace elements

Lithophile trace elements enriched (3x the background value) in all altered rocks include Ba, Cs, Rb and W, tungsten in scheelite up to the per cent level. Sr is enriched in both magnesian gold skarns, and Ni in the East Lode almandine-biotite schist. Lithium is enriched in the Boulder Lode bulk ore and in the East Lode biotite gneiss (ESM Figs. 1b, d).

Comparison of the chalcophile trace element patterns is limited to concentrations above the detection limit (Table 1). Gold, As (in loellingite, arsenopyrite) and Pb (in galena) are enriched in all altered rocks. Sb is enriched in four samples but below detection in the East Lode gneiss (MLO-72), which is low in arsenic (Table 1). In the sulfide-rich samples (ESM Figs. 1a-d), Ag is consistently enriched, too. In the bulk quartz-diopside ore of the Boulder Lode, the elements Bi, Mo, Te and Zn are selectively enriched (ESM Fig. 1b), detected at low concentrations except for Zn but well above background (Table 1).

Discussion

Most skarn deposits mined for metals (Fe, Cu, Zn-Pb, W, Mo, Sn, Au) are related to diorite-granite intrusions (Smirnov 1976; Einaudi et al. 1981). The magmatic fluid infiltrating the host rocks precipitates silicates, oxides, sulfides and gold during the evolution from early high-T (650–500 °C) to late retrograde hydrothermal conditions (500–350 °C; Meinert 1998; Rubin and Kyle 1998). Below, we discuss the PTX-constraints on skarn formation and sulfide deposition in the East, Boulder and Savage Lodes of the Marvel Loch deposit based on new results compiled in the ESM and on published data. A discussion of the mass-balance and isotopic data tracing the fluid source precedes short comparisons to Precambrian "orogenic" deposits similar to Marvel Loch, and to Phanerozoic W-Au skarns.

Pressure constraints

The pressure estimates of 400 MPa during amphibolite-facies metamorphism in the aureole of the Ghooli Dome batholith (Gole and Klein 1981; Dalstra et al. 1998), the estimate of 370 MPa for skarn formation at Marvel Loch (Mueller et al. 1991), and the assemblage spodumene + quartz (300–400 MPa; London 1984) in LCT pegmatites at Southern Cross equate to a crustal depth of 11–15 km at lithostatic load (Spear 1993). Assuming a geothermal gradient of 30 °C/km in the crust (Barton and Hanson 1989), this depth results in an ambient temperature of 350–400 °C, the minimum the skarn-forming fluid at Marvel Loch could cool to.

Magmatic fluids exsolved at 300–400 MPa pressure contain carbon dioxide, as reviewed in Lowenstern (2001) and Mueller (2025). At Marvel Loch, inclusions in East Lode quartz-diopside veins contained H_2O-CO_2 fluid with CH_4/CO_2 molar ratios < 0.15. Homogenisation temperature and salinity could not be determined due to post-entrapment modification (Ridley and Hagemann 1999). In the nearby Nevoria deposit, inclusions in grossular, diopside and quartz contained a low to moderate salinity (0.1–10 wt% NaCl $_{eq}$) H_2O-CO_2 ± CH_4 fluid with minor $CaCl_2$ and $MgCl_2$. The data indicate a minimum X_{CO2} = 0.1 in the fluid phase, low CH_4/CO_2 ratios in amphibolite-hosted skarn and high but variable CH_4/CO_2 in reduced gold skarn replacing grunerite-quartz BIF (Fan et al. 2000).

Temperature constraints

A pressure of 400 MPa is assumed for skarn formation at Marvel Loch based on the constraints outlined above. Apparently, there was little uplift and erosion in the continental foreland of the EG orogen during the period 2775 − 2620 Ma lasting from the emplacement of the Ghooli Dome batholith to the intrusion of post-orogenic Li-Cs-Ta pegmatites.

East Lode The early-stage assemblage in almandine-biotite schist at the margin of the East Lode gold skarn and skarn-banded gneiss provides reliable temperature estimates (ESM Table 2a). Both the garnet ($alm_{88–90}$,$prp_{5–6}$) and biotite (mainly annite, $Mg/Mg+Fe^{2+}$ = 0.17–0.23) are iron-rich. In the end-member KFASH system, the assemblage almandine + biotite + staurolite (Fig. 10c) constrains temperature to 550–620 °C at 400 MPa (Fig. 2). The average Mg-Fe^{2+} exchange temperature of garnet-biotite pairs is 645 ± 50 °C (n = 3) using the calibration of Perchuk and Lavrent'eva (1983), and 641–659 °C (n = 2, rim assemblages only) using that of Ferry and Spear (1978). As the Mössbauer spectroscopy of the almandine-biotite schist detected 4.22 wt% Fe_2O_3 in the whole rock, the temperatures above have been calculated by assigning this amount to biotite (Fe^{3+}/Fe_{total} = 0.13–0.15), a minimum given that the co-existing phases (almandine, quartz, oligoclase, tourmaline, ilmenite) do not contain significant ferric iron. The corrected garnet-biotite exchange temperatures agree with the independent estimate of 651 ± 50 °C (n = 3) using the Ti-in-biotite calibration of Henry et al. (2005). The Fe-rich biotites are outside the empirical range of the Wu and Chen (2015) thermometer. Both Ti-in-biotite calibrations assume a ratio Fe^{3+}/Fe_{total} = 0.12, slightly above the absolute minimum of 0.1 (Dachs and Benisek 2015), even in biotite from highly reduced host rocks. The Wu and Chen (2015) thermometer provides reliable estimates for annite-phlogopite micas ($Mg/Mg+Fe^{2+}$ = 0.47–0.62) from the diopside-hornblende gold skarn (615 °C), and from the skarn-banded gneiss (556–565 °C) resulting in an average of 579 ± 65 °C (n = 3) for the sulfide-rich units of the East Lode (ESM Table 2e).

Boulder Lode The assemblages quartz + diopside + calcite, quartz + actinolite + calcite and actinolite + calcite, and rare interstitial anorthite + microcline indicate temperatures of 600–500 °C at X_{CO2} = 0.1 in the fluid phase (Fig. 7 in Mueller et al. 1991). Most of the quartz-diopside ore probably formed when the fluid cooled below 550 °C, as the solubility of SiO_2 decreases sharply with temperature at 300–400 MPa pressure (Holland and Malinin 1979). Quartz replacement of outer tremolite-phlogopite-chlorite skarn continued into the retrograde phase at 500–400 °C (Fig. 12).

Savage Lode In the calcite-rich Savage Lode, petrogenetic grids, the EPMA data of mineral assemblages, and calcite-dolomite solvus thermometry indicate cooling of an aqueous-carbonic fluid (X_{CO2} = 0.10–0.15) from a peak of 640 ± 20 °C at 350–400 MPa (olivine-calcite-spinel-chlorite) to 610–540 °C during calcite ± dolomite and magnetite deposition. The intermediate-stage assemblage calcite + chlorite + phlogopite provides a lower limit of 450 °C (Mueller et al. 1991). These estimates are supported by the application of the Wu and Chen (2015) Ti-in-biotite thermometer to phlogopite (ESM Table 3), and by the olivine-ilmenite Mg-Fe^{2+} exchange thermometer of Andersen and Lindsley (1979) to oxide assemblages in olivine-calcite skarn (ESM Table 5). Phlogopites from the Savage Lode and from outer olivine-bearing tremolite-chlorite skarn gave temperatures of 487 ± 65 °C (n = 3) and 492 ± 65 °C (n = 4), respectively. The estimates for olivine-ilmenite assemblages in the Savage Lode are 624 ± 30 °C for high-Mg ilmenite, and 582 ± 30 °C for the average ilmenite in three out of four oxide aggregates analyzed. Low-Mg ilmenite in one aggregate gave 453 ± 30 °C, a temperature outside the calibration range of Andersen and Lindsley (1979) and at the lower limit of calcite-chlorite-phlogopite stability.

Outer and retrograde skarn Gradients to lower X_{CO2} in the hydrothemal fluid (X_{CO2} < 0.05) are evident in the lack of carbonate in outer prograde skarn containing the Savage Lode (Mueller 1991), and in the evolution from early to late skarn assemblages (Mueller et al. 1991). Retrograde lizardite + chrysotile after olivine and talc after tremolite in magnesian skarn, and phengite-clinozoisite-prehnite aggregates after anorthite in the East Lode formed when the temperature fell to about 400 °C. The upper thermal stability of hydrothermal chrysotile is 470 °C (Deer et al. 2009), and that of prehnite 400 °C (Liou 1971; Liou et al. 1983). In the metamorphic rocks distal to the gold ore bodies,

replacement zones of serpentine-magnetite ± talc in meta-komatiite, and of chlorite-phengite-prehnite in meta-gabbro reflect the infiltration of cooler aqueous hydrothermal fluid away from the up-flow zone at the lithologic contact. The evolution to low-T minerals indicates that the hydrothermal system cooled to the ambient temperature at 11–15 km depth in the terrane. The system is post-metamorphic, as the peak temperature of aureole metamorphism at Marvel Loch is estimated at 650 ± 50 °C.

Fluid oxidation state

In the early-stage almandine-biotite schist bordering the East Lode, the oxygen fugacity may be estimated using the assemblage Fe-biotite + quartz and the log f_{O2} versus temperature diagram of Eugster and Wones (1962). At 650–600 °C and 207 MPa, the upper boundary of the annite + quartz stability field defines a maximum log f_{O2} of -18 to -19 bar, and the lower boundary a minimum of -21 to -24 bar (Fig. 13a). As the assemblage K-feldspar + quartz + magnetite limiting the upper boundary is present in the almandine-grossular gneiss bordering the schist (Figs. 9 and 10a), and the pressure during skarn formation was higher (400 MPa), the estimate of log f_{O2} = -18 to -19 bar during formation of the two outer garnet-bearing units of the East Lode is reasonable but probably a minimum.

The ilmenite in Savage Lode olivine-calcite skarn is hematite-free (< 1 mol% Fe_2O_3), more reduced than the product ilmenite (1–6 mol%) of Andersen and Lindsley (1979). Considering their experiments, which also lacked Ti-magnetite as a reaction product, the early assemblage olivine + ilmenite + Mg-Fe spinel suggests an upper limit for oxygen fugacity close to the Co-CoO buffer (log f_{O2} = -19 bar at 640 °C and 400 MPa; Frost 1991), the buffer they used for f_{O2}-control. Magnetite with no ulvöspinel component would precipitate in the calcite-rich ore due to an increase in oxygen fugacty or, alternatively, when temperature fell to < 550 °C, if the oxygen fugacity was maintained

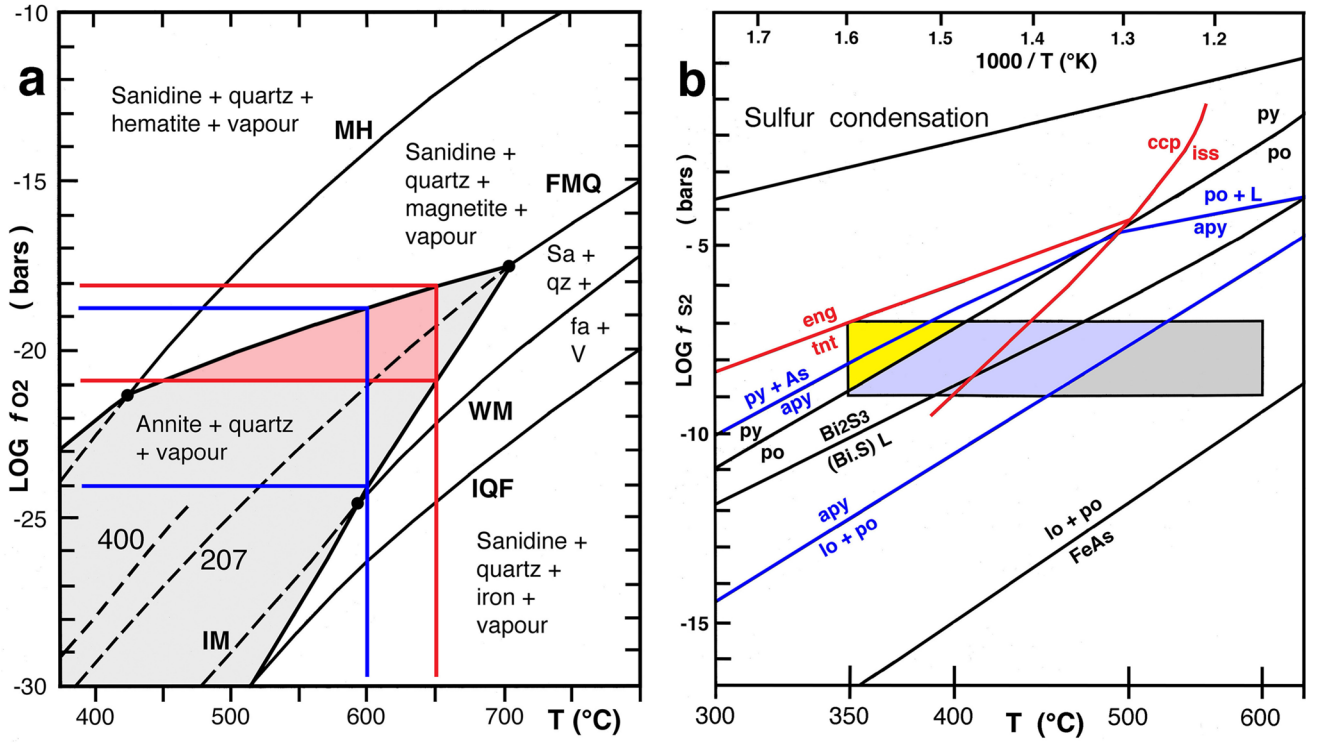

Fig. 13 Oxygen and sulfur fugacity versus temperature diagrams constraining the oxidation and sulfidation state of gold skarn in the Marvel Loch deposit. **a** Log f_{O2} – T diagram (modified from Fleet 2003) showing the stability of Fe-biotite (annite) + quartz (grey field) in early-stage almandine-biotite schist of the East Lode based on experimental data in Eugster and Wones (1962) at 207 MPa. The red field illustrates the oxygen fugacity at 650 °C. A fluid oxygen fugacity of log f_{O2} = -18 bar is consistent with the higher pressure (400 MPa) and the upper-limit assemblage microcline + quartz + magnetite in the adjacent garnet gneiss. **b** Log f_{S2} – T diagram (modified from Barton and Skinner 1979) illustrating sulfide deposition in Marvel Loch gold skarns at a sulfur fugacity of 10^{-7} to 10^{-9} bar (Mueller et al. 1991). Sulfidation reactions constraining the stability of arsenopyrite are in blue, those of chalcopyrite and tennantite in red. Loellingite + pyrrhotite (grey field), arsenopyrite + pyrrhotite (blue field), and pyrrhotite + pyrite ± arsenopyrite (yellow field) were deposited during cooling from about 600 °C to 350 °C. Arsenopyrite (apy), bismuthinite (Bi_2S_3), bismuth-rich melt ([Bi.S] L), chalcopyrite (ccp), enargite (eng), intermediate solid solution (iss), loellingite (lo), pyrrhotite (po), pyrite (py), tennantite (tnt)

by the infiltrating fluid at about $\log f_{O2}$ = -19 bar. Such evolving conditions are indicated by the replacement of ilmenite and spinel by magnetite.

Fluid reduction

There is indirect evidence for the reduction of the hydrothermal fluid during large-scale greenstone replacement. In the quartz-diopside vein at the margin of the Savage Lode, the carbonic phase in fluid inclusions varied from pure CO_2 to almost pure CH_4 (Ridley and Hagemann 1999) suggesting a reduction of CO_2, consistent with the Fe^{3+}/Fe_{total} ratio (0.201) of the calcite-rich ore relative to the low ratio (0.031) of outer diopside skarn (Mueller 1991). The positive europium anomalies in the chondrite-normalized REE patterns of scheelite from the Boulder and East Lode gold skarns (ESM Fig. 2) suggest reducing conditions at the site of crystallization, as Eu^{2+} substitutes more readily for Ca^{2+} in the tetragonal scheelite lattice than the smaller trivalent REE ions (Hsu 1981; Brookins 1989).

Gold and sulfide deposition

In the Savage Lode, Ni-rich loellingite (10.6 at% Ni) and native gold low in silver (ESM Table 4) crystallized early in high-T olivine-calcite skarn. Hem and Makovicky (2004) synthesized loellingite with 11 at% Ni at 650 °C, and loellingite with only 0.8 at% Ni at 500 °C, both in equilibrium with arsenopyrite. High-T pyrrhotite contains up to 3 at% Cu (Barton and Skinner 1979). In Savage Lode ore, pyrrhotite and loellingite are in contact with small grains of chalcopyrite and niccolite, respectively, probably exsolved from the high-T phases. Textural relations and thermometry indicate that most pyrrhotite, loellingite, minor arsenopyrite, and gold (?) precipitated when the fluid cooled to 500 °C at about constant sulfur fugacity (Fig. 13b).

In magnesian skarn of the Boulder and Undaunted Lodes, grains of silver-rich gold are enclosed in quartz and diopside. Loellingite is rare or absent. Arsenopyrite, hexagonal pyrrhotite, and galena-sphalerite-chalcopyrite-tennantite aggregates are in contact with Au-Ag alloy. Fe-rich sphalerite contains blebs of chalcopyrite. Both sulfides are in solid solution and thus incompatible above 500 °C (Barton and Skinner 1979; Bowles et al. 2011) suggesting that the base-metal sulfides crystallized at 500–400 °C (Fig. 13b). Drop-shaped native bismuth occurs enclosed in galena, and native bismuth with thin rims of pure gold is enclosed in quartz or attached to sulfide aggregates (Fig. 8). Native bismuth has a low melting point (241 °C at 400 MPa; Barton and Skinner 1979). The textures indicate the transport of bismuth melt droplets in the fluid, the scavenging of gold by suspended droplets (Tooth et al. 2011), and the unmixing of the Bi-Au alloy during terrane cooling.

The lithologic contact meta-gabbro / meta-komatiite controlled intense sulfide deposition in skarn-banded East Lode gneiss. Here, the dioside-hornblende gold skarn is mineralized with arsenopyrite, pyrrhotite, galena, chalcopyrite, and silver-rich gold, the same assemblage as in magnesian skarn of the Boulder Lode except for the greater abundance of pyrite and the occurrence of marcasite. Marcasite transforms to the cubic FeS_2 phase at >425 °C via a solid-state process (Fleet 1970). In the low-grade East Lode gneiss (0.3–0.4 g/t Au), the assemblage pyrrhotite + pyrite is predominant. The retrogression of anorthite to phengite + clinozoisite + prehnite suggests pyrite-marcasite deposition at 450–350 °C (Fig. 13b), the estimated ambient temperature in the terrane. Sulfur fugacity varied close to the pyrite-pyrrhotite equilibrium as indicated by pyrrhotite rimming pyrite.

Fluid source

At Marvel Loch, the downward kink in a branch of the southern pegmatite at the shear-zone boundary and structures in foliated skarn indicate coeval intrusive and hydrothermal activity during reverse-dextral movement in the contact alteration zone. Native gold and arsenopyrite in sericite-chlorite altered albite pegmatite enclosed in skarn suggest emplacement of the southern dike during retrograde alteration and mineralization (Mueller 1991). Other dikes crosscut skarn, consistent with multiple phases of intrusion at ca. 2630 Ma. The setting is similar to that at Nevoria, where the gold skarn (2635.7 ± 1.2 Ma) and the pegmatite-granite complex (2634 ± 4 Ma) are coeval within error of the U-Pb ages (Mueller et al. 2004).

The pegmatitic granite at 650–800 m depth below the Marvel Loch deposit is implicated as the source by the $\delta^{13}C_{PDB}$ ratio of CO_2 (-5.5 to -4.6‰) in the fluid of the Savage Lode (Mueller et al. 1991). These values are typical of magmatic carbon (-5 to -8‰) in I-type intrusion-related skarn systems (Shimazaki et al. 1986; Bowman 1998). The initial $^{87}Sr/^{86}Sr$ ratios of scheelite (0.7024) and the $^{206}Pb/^{204}Pb$ ratios of galena (13.768) in skarn are higher than those of the mantle-derived host rocks (0.7001, 13.382; Mueller et al. 1991). The ratios represent the fluid isotope composition at the site of crystallization, evolved as a result of Sr and Pb exchange with the host rocks (Ridley and Diamond 2000). However, the $^{87}Sr/^{86}Sr$ ratios in scheelite from gold skarns in the SCB increase from distal to proximal deposits, and overlap with the initial values of post-orogenic I-type granites (Mueller 2025).

Apart from CO_2, Sr and Pb, the granite complex is the most likely source of Ca, K, Ba, Cs, Rb and Li in the alteration zone (ESM Fig. 1). In Marvel Loch gold ore, there is a pervasive enrichment of W and As, and an enrichment

of Bi in quartz-diopside skarn. All three elements are also enriched in the roof pegmatite (As 9 ppm, Bi 14 ppm, W 6 ppm) of the zoned Nevoria granite (Mueller et al. 2004) relative to concentrations in granite world-wide (As 0.5 ppm, Bi 0.07 ppm, W 0.4 ppm; Krauskopf and Bird 1995). Fluid released from the Greenbushes spodumene pegmatite, SW Yilgarn Craton, caused Li enrichment in the host greenstones more than 150 m, and Rb-Cs-As enrichment up to 100 m away from the intrusive contact (Sweetapple et al. 2024).

Orogenic hypozonal gold

The magnesian gold skarns at Marvel Loch are not unique but have counterparts at Yilgarn Star (34 t Au) in the Southern Cross Belt (Witt et al. 2001), and in the Tucano deposit (56 t Au; 400–500 MPa, 600–480 °C) in greenstones of the Guiana Craton, Brazil (Soares et al. 2025). Both are classified as "hypozonal orogenic", a term applied to deposits formed at continental margins in crustal-scale shear zones at >12 km depth (Groves et al. 1998; Goldfarb et al. 2005). Metamorphic H_2O-CO_2 fluids released in the lower continental crust are invoked as the source of gold (Goldfarb and Pitcairn 2023). The ore bodies in the Tucano olivine-calcite "marble" share details with the Savage Lode including the gangue, the presence of Mg-Fe spinel and magnetite, the pyrrhotite-loellingite ± arsenopyrite assemblage, and the spatial relationship to garnet-muscovite granite and pegmatite, the diagnostic intrusions associated with the Marvel Loch and Nevoria skarn deposits.

Reduced W-Au skarns

Sub-volcanic Au ± Cu skarns are related to I-type, magnetite- or ilmenite-series porphyry stocks emplaced at 1–5 km depth below cogenetic volcanic fields (Meinert 2000), a high-level setting not comparable to that at Marvel Loch. In contrast, reduced tungsten skarns (0.7–1.9 g/t Au; Newberry 1998) are associated with granodiorites and granites emplaced at 6–10 km depth (130–250 MPa; typically 200 MPa) in continental plutonic arcs (Einaudi et al. 1981; Newberry 1998). The associated plutons are characterized by K-feldspar megacrysts, interstitial quartz-feldspar myrmekite, and garnet-muscovite pegmatite. Most classify as I-type ilmenite-series with oxidation states between the NNO and QFM buffers (Ohmoto 1986; Newberry 1998).

The hornfels-marble successions hosting reduced tungsten deposits are carbonaceous (Dick and Hodgson 1982). Anhydrous grossular-hedenbergite skarn (600–500 °C) in marble is partly overprinted by almandine-spessartine garnet, and by hydrous amphibole-, biotite- and chlorite-pyrrhotite replacement enriched in scheelite (Newberry 1983, 1998). The lower Véronique SE ore body in the Permian Salau deposit, France, averaged 10 g/t Au in actinolite-pyrrhotite-arsenopyrite skarn, where native gold was associated with galena, Bi-selenides, native bismuth, bismuthinite, hessite and tetradymite (Fonteilles et al. 1989). Hydrous skarn in the Cretaceous Cantung deposit, Yukon, Canada, was enriched in electrum, native bismuth, Bi-tellurides, and Bi-Te selenides (Lentz et al. 2017).

Conclusions

(1) The term "orogenic" does not apply to gold deposits such as Marvel Loch and Nevoria, which are located outside the 2.7 Ga Eastern Goldfields orogen in its continental foreland. Both deposits postdate amphibolite-facies aureole metamorphism in the 3.0 Ga greenstone belt by 90–140 Ma.

(2) The Marvel Loch deposit is not controlled by a crustal-scale, strike-slip shear zone. Instead, the foliated alteration zone at the vertical contact of a meta-gabbro sill records reverse-dextral movement, the SW-side lifted up during the emplacement of the associated pegmatite complex.

(3) Post-orogenic garnet-muscovite pegmatites were emplaced at ca. 2630 Ma southwest of the contact-bound gold skarns, and below the ore bodies at 650–800 m depth. Structural relations and gold in pegmatite suggest multiple phases of intrusive activity coeval with mineralization.

(4) The metasomatic enrichment of CaO, CO_2, K_2O, Ba, Cs, Rb, Li, Sr, Pb, W and As in the calcic-potassic alteration zone, and the carbon, strontium and lead isotopic data of ore-related calcite, scheelite and galena implicate the pegmatitic granite below the Marvel Loch deposit as the source of the high-T (up to 650 °C) auriferous fluid. An I-type magmatic source is indicated by the carbon-isotope signature ($\delta^{13}C_{PDB}$ = -4.8‰) of CO_2 in the aqueous fluid of the Savage Lode.

(5) The Au-Ag ore bodies at Marvel Loch are classified as magnesian or calcic skarns, because the high-T gangue contains native gold, and consists of minerals typical of magnesian (olivine, diopside, spinel) or calcic skarn deposits (diopside, hornblende, anorthite). Skarn composition was influenced by the host rock replaced: meta-komatiite (21 wt% MgO) and meta-gabbro (5.6% MgO).

(6) Fluid cooling combined with reduction caused the deposition of gold in skarn silicates. Gold and low-sulfidation sulfide-arsenide assemblages precipitated during cooling at an estimated sulfur fugacity of 10^{-7} to 10^{-9} bar: pyrrhotite + Ni-loellingite at 650–500 °C in calcite-rich skarn, arsenopyrite + pyrrhotite + base-metal sulfides ± tennantite ± bismuth at 550–400 °C in quartz-diopside skarn, and pyrrhotite + pyrite ± marcasite at 450–350 °C in skarn-banded gneiss at the meta-gabbro contact.

The Marvel Loch high-T deposit in the Southern Cross greenstone belt represents an intrusion-related gold skarn system formed at 11–15 km depth (300–400 MPa) in a batholith environment comparable to that of W-Au skarns (200–250 MPa). The W-Au-As-Bi geochemical signature shared by Marvel Loch and reduced tungsten skarns may reflect the oxidation state of the related intrusion (I-type ilmenite-series?), and fluid cooling plus reduction during the infiltration of ferrous or graphitic host rocks.

Supplementary Information The online version contains supplementary material available at https://doi.org/10.1007/s00126-026-01448-1.

Acknowledgements An early version of this study remained unfinished for medical reasons, which diminished my eye sight during the period 1998–2005. The author is grateful to Larry Meinert for his introduction to skarn geology during his PhD study at the University of Western Australia, and to Marco Einaudi for sharing his knowledge on skarns and other intrusion-related ore deposits. Constructive criticism by Nils Jansson and John Walshe, and comments by Larry Meinert and an anonymous referee helped to improve the manuscript. My wife Ute used her mathematical skills to test the Andersen and Lindsley (1979, 1981) and Wu and Chen (2015) geothermometers.

Funding Open Access funding enabled and organized by Projekt DEAL.

Data availability All data are accessible in the manuscript and in the Supplementary Material.

Declarations

Conflict of interest The author declares no conflict of interest.

References

Ahmat AL (1986) Metamorphic patterns in the greenstone belts of the Southern Cross Province, Western Australia. Geol Surv Western Australia, Prof Paper 19: 1–21

Andersen DJ, Lindsley DH (1979) The olivine-ilmenite thermometer. Proc Lunar Planet Sci Conf 10:493–507

Barton MD, Hanson RB (1989) Magmatism and the development of low-pressure metamorphic belts: Implications from the western United States and thermal modeling. Geol Soc Am Bull 101:1051–1065

Barton PB, Skinner BJ (1979) Sulfide mineral stabilities. In: Barnes HL (ed) Geochemistry of hydrothermal ore deposits, 2nd edn. Wiley, New York, pp 278–403

Bettenay LF (1977) Regional geology and petrogenesis of Archaean granitoids in the southeastern Yilgarn Block, Western Australia. Dissertation, the University of Western Australia, Perth

Blatchford T (1915) The geology and mineral resources of the Yilgarn Goldfield Part 2. The gold belt south of Southern Cross. Geol Surv West Australia Bull 63:1–189

Bohlen SR, Montana A, Kerrick DM (1991) Precise determinations of the equilibria kyanite-sillimanite and kyanite-andalusite and a revised triple point for Al_2SiO_5 polymorphs. Am Mineral 76:677–680

Bowles JFW, Howie RA, Vaughan DJ, Zussman J (2011) Non-silicates: oxides, hydroxides and sulphides. Rock-forming minerals Vol 5A, 2nd edn. The Geological Society, London

Bowman JR (1998) Stable-isotope systematics of skarns. In: Lentz DR (ed) Mineralized intrusion-related skarn systems. Min Ass Canada, Short Course 26: 99–145

Brabham JR (1995) Field excursion guide to Marvel Loch gold mine, supplement to Schwebel PJ (ed) Southern Cross greenstone belt, geology and gold mines. Perth, Western Australia, Geoconferences Inc

Brabham JR, Johnson N (1995) Marvel Loch gold mine. In: Schwebel PJ (ed) Southern Cross greenstone belt, geology and gold mines, pp. 81–84. Perth, Western Australia, Geoconferences Inc

Brookins DG (1989) Aqueous geochemistry of rare earth elements. In: Lipin BR, McKay GA (eds) Geochemistry and mineralogy of rare earth elements. Min Soc Am, Rev Mineralogy 21: 201–225

Bucher K, Frey M (2002) Petrogenesis of metamorphic rocks, 7th edn. Springer, Berlin, pp 1–341

Carroll D (1939) Sand-plain soils from the Yilgarn Goldfield, In: Ellis HA (ed) The geology of the Yilgarn Goldfield, south of the Great Eastern railway, Appendix. Geol Surv West Australia Bull 97: 161–179

Chen SF, Riganti A, Wyche S, Greenfield JE, Nelson DR (2003) Lithostratigraphy and tectonic evolution of contrasting greenstone successions in the central Yilgarn Craton, Western Australia. Precambrian Res 127:249–266

Côté-Mantha O, Daigneault R, Gaboury D, Chartrand F, Pilote P (2012) Geology, alteration, and origin of Archean Au-Ag-Cu mineralization associated with the synvolcanic Chibougamau pluton: the Brosman prospect, Abitibi greenstone belt. Econ Geol 107:909–934

Dachs E, Benisek A (2015) Standard-state thermodynamic properties of annite, $KFe_3[(OH)_2AlSi_3O_{10}]$, based on new calorimetric measurements. Eur J Mineral 27:603–616

Dalstra HJ, Bloem EJM, Ridley JR, Groves DI (1998) Diapirism synchronous with regional deformation and gold mineralization, a new concept for granitoid emplacement in the Southern Cross Province, Western Australia. Geol Mijnbouw 76:321–338

Deer WA, Howie RA, Zussman J (2009) Layered silicates excluding micas and clay minerals. Rock-forming Minerals 3B, 2nd edition. The Geological Society London

Deer WA, Howie RA, Zussman J (2013) An introduction to the rock-forming minerals, 3rd edition. London, Mineralogical Society

Dick LA, Hodgson CJ (1982) The Mac Tung W-Cu (Zn) contact metasomatic and related deposits of the northeastern Canadian cordillera. Econ Geol 77:845–867

Doublier MP, Thebaud N, Wingate MTD, Romano SS, Kirkland CL, Gessner K, Mole DR, Evans N (2014) Structure and timing of Neoarchean gold mineralization in the Southern Cross district (Yilgarn Craton, Western Australia) suggest leading role of late low-Ca I-type granite intrusions. J Struc Geol 67:205–221

Einaudi MT, Burt DM (1982) Terminology, classification, and composition of skarn deposits. Econ Geol 77:745–754

Einaudi MT, Meinert LD, Newberry RJ (1981) Skarn deposits. Econ Geol 75th Anniversary Vol, 317–391

Ellis HA (1939) The geology of the Yilgarn Goldfield, south of the Great Eastern railway. Geol Surv West Australia Bull 97:1–160

Eugster HP, Wones D (1962) Stability relations of the ferruginous biotite, annite. J Petrol 3:82–125

Fan HR, Groves DI, Mikucki EJ, McNaughton NJ (2000) Contrasting fluid types at the Nevoria gold deposit in the Southern Cross greenstone belt, Western Australia: Implications of auriferous fluids depositing ores within an Archean banded iron-formation. Econ Geol 95:1527–1536

Ferry JM, Spear FS (1978) Experimental calibration of the partitioning of Fe and Mg between biotite and garnet. Contrib Miner Petrol 66:113–117

Fleet ME (1970) Structural aspects of the marcasite-pyrite transformation. Can Mineral 10:225–231

Fleet ME (2003) Sheet silicates: Micas. Rock-forming minerals, Vol 3A, 2nd edn. The Geological Society London

Fonteilles M, Soler P, Demange M, Derré C, Krier-Schellen AD, Verkaeren J, Guy B, Zahm A (1989) The scheelite skarn deposit of Salau (Arriege, French Pyrenees). Econ Geol 84:1172–1209

Frost BR (1991) Introduction to oxygen fugacity and its petrologic importance. In: Lindsley DH (ed) Oxide minerals: petrologic and magnetic significance. Min Soc America, Rev in Mineralogy 25:1–9

Goldfarb RJ, Pitcairn I (2023) Orogenic gold: is a genetic association with magmatism realistic? Miner Deposita 58:5–35

Goldfarb RJ, Baker T, Dubé B, Groves DI, Hart CJR, Gosselin P (2005) Distribution, character, and genesis of gold deposits in metamorphic terranes. Econ Geol 100th Anniversary Vol, 407–450

Gole MJ, Klein C (1981) High-grade metamorphic Archaean banded iron-formation, Western Australia: assemblages with coexisting pyroxenes ± fayalite. Am Mineral 66:87–99

Grant JA (1986) The isocon diagram -- a simple solution to Gresen's equation for metasomatic alteration. Econ Geol 81:1976–1982

Groves DI, Goldfarb RJ, Gebre-Mariam M, Hagemann SG, Robert F (1998) Orogenic gold deposits: a proposed classification in the context of their crustal distribution and relationship to other deposit types. Ore Geol Rev 13:7–27

GSWA, Geological Survey of Western Australia (2005) Southern Cross, Sheet SH 50 – 16. Western Australia 1:250 000 Total Magnetic Intensity Image

Hallberg JA (1987) Postcratonization mafic and ultramafic dikes of the Yilgarn Block. Aust J Earth Sci 34:135–149

Hem SR, Makovicky E (2004) The system Fe-Co-Ni-As-S. II. Phase relations in the (Fe, Co, Ni)$As_{1.5}S_{0.5}$ section at 650° and 500°C. Can Mineral 42:63–86

Henry DJ, Guidotti CV, Thomson JA (2005) The Ti-saturation surface for low- to medium-pressure metapelitic biotites: Implications for geothermometry and Ti-substitution mechanisms. Am Mineral 90:316–328

Holland T, Blundy J (1994) Non-ideal interactions in calcic amphiboles and their bearing on amphibole-plagioclase thermometry. Contr Mineral Petrol 116:433–447

Holland HD, Malinin SD (1979) The solubility and occurrence of non-ore minerals. In: Barnes HL (ed) Geochemistry of hydrothermal ore deposits, 2nd edition, pp. 461–508. Wiley & Sons, New York

Hsu LC (1981) Phase relations of some tungstate minerals under hydrothermal conditions. Am Mineral 66:298–308

IMA, International Mineralogical Association (1989) Nomenclature of pyroxenes. Can Mineral 27:143–156

IMA, International Mineralogical Association (1997) Nomenclature of amphiboles: Report of the subcommittee on amphiboles of the International Mineralogical Association, Commission on new minerals and mineral names. Can Mineral 35:219–246

IMA, International Mineralogical Association (1998) Nomenclature of the micas. Can Mineral 36:905–912

Keats W (1991) Geology and gold mines of the Bullfinch-Parker Range region, Southern Cross province, Western Australia. Geol Surv West Australia Rept 28:1–44

Krauskopf KB, Bird DK (1995) Introduction to geochemistry, 3rd edn. McGraw-Hill, Boston, New York

Lentz CPE, McFarlane CRM, Falck H (2017) Physiochemical controls on gold mineralization in the Amber Zone at the Cantung mine, N.W.T. Mineral resources to discover – 14th SGA Biennial Meeting 2017, Quebec City, Ext Abstr 1: 315–318

Libby JW, Groves DI, Vearncombe JR (1991) The nature and tectonic significance of the crustal-scale Koolyanobbing shear zone, Yilgarn craton, Western Australia. Aust J Earth Sci 38:229–245

Liou JG (1971) Synthesis and stability relations of prehnite, $Ca_3Al_2Si_3O_{10}(OH)_2$. Am Mineral 56:507–531

Liou JG, Kim HS, Maruyama S (1983) Prehnite-epidote equilibria and their petrologic applications. J Petrol 24:321–342

London D (1984) Experimental phase equilibria in the system LiAlSiO_4-SiO_2-H_2O: a petrogenetic grid for lithium-rich pegmatites. Am Mineral 69:995–1004

Lowenstern JB (2001) Carbon dioxide in magmas and implications for hydrothermal systems. Miner Deposita 36:490–502

Matheson RS, Hobson RA (1940) The mining groups of the Yilgarn Goldfield south of the Great Eastern railway, Part 1. Geol Surv Western Austr Bull 98:1–165

Meinert LD (1998) A review of skarns that contain gold. In: Lentz DR (ed) Mineralized intrusion-related skarn systems. Min Ass Canada, Short Course 26: 359–414

Meinert LD (2000) Gold in skarns related to epizonal intrusions. Rev Econ Geol 13:347–375

Meinert LD, Dipple GM, Nicolescu S (2005) World skarn deposits. Economic Geology 100th Anniversary Vol, 299–336

Mueller AG (1988) Archaean gold-silver deposits with prominent calc-silicate alteration in the Southern Cross greenstone belt, Western Australia: Analogues of Phanerozoic skarn deposits. In Ho SE, Groves DI (eds) Advances in Understanding Precambrian Gold Deposits, Volume 2. Perth, Univ Western Australia Publ 12: 141–163

Mueller AG (1990) The nature and genesis of high- and medium-temperature Archaean gold deposits in the Yilgarn Block, Western Australia, including a specific study of scheelite-bearing gold skarn deposits: Dissertation, The University of Western Australia

Mueller AG (1991) The Savage Lode magnesian skarn in the Marvel Loch gold-silver mine, Southern Cross greenstone belt, Western Australia: Part I. Structural setting, petrography and geochemistry. Can J Earth Sci 28:659–685

Mueller AG (1997) The Nevoria gold skarn deposit in Archean iron-formation, Southern Cross greenstone belt, Western Australia: I. Tectonic setting, petrography, and classification. Econ Geol 92:181–209

Mueller AG (2025) Granite-pegmatite-related gold skarns and associated Li-Cs-Ta pegmatites in the Archean Yilgarn Craton, Western Australia. Miner Deposita 60:835–867

Mueller AG (2026) Reply to the discussion on Granite-pegmatite-related gold skarns and associated Li-Cs-Ta pegmatites in the Archean Yilgarn Craton, Western Australia by Witt (2025). Miner Deposita 61:973–977

Mueller AG, Groves DI (1991) The classification of Western Australian greenstone-hosted gold deposits according to wallrock-alteration mineral assemblages. Ore Geol Rev 6:291–331

Mueller AG, McNaughton NJ (2000) U-Pb ages constraining batholith emplacement, contact metamorphism, and the formation of gold and W-Mo skarns in the Southern Cross area, Yilgarn Craton, Western Australia. Econ Geol 95:1231–1257

Mueller AG, Groves DI, Delor CP (1991) The Savage Lode magnesian skarn in the Marvel Loch gold-silver mine, Southern Cross greenstone belt, Western Australia: Part II. Pressure-temperature estimates and constraints on fluid sources. Can J Earth Sci 28:686–705

Mueller AG, Nemchin AA, Frei R (2004) The Nevoria gold skarn deposit, Southern Cross greenstone belt, Western Australia: II. Pressure-temperature-time path and relationship to postorogenic granites. Econ Geol 99:453–478

Mueller AG, Hagemann SG, McNaughton NJ (2020) Neoarchean orogenic, magmatic and hydrothermal events in the Kalgoorlie-Kambalda area, Western Australia: constraints on gold mineralization in the Boulder Lefroy-Golden Mile fault system. Miner Deposita 55:633–663

Newberry RJ (1983) The formation of subcalcic garnet in scheelite-bearing skarns. Can Mineral 21:529–544

Newberry RJ (1998) W- and Sn-skarn deposits: A 1998 status report. In: Lentz DR (ed) Mineralized intrusion-related skarn systems. Min Ass Canada, Short Course 26: 289–335

Ohmoto H (1986) Stable isotope geochemistry of ore deposits. In: Valley JW, Taylor HP jr, O'Neil JR (eds) Stable isotopes in high temperature geological processes. Min Soc America, Rv Mineralogy 16: 491–560

Perchuk LL, Lavrenteva IV (1983) Experimental investigation of exchange equilibria in the system cordierite-garnet-biotite. In: Saxena SK (ed) Kinetic and equilibrium in mineral reactions. Springer, New York, pp 199–239

Qiu YM, McNaughton NJ, Groves DI, Dalstra HJ (1999) Ages of internal granitoids in the Southern Cross region, Yilgarn Craton, Western Australia, and their crustal evolution and tectonic implications. Aust J Earth Sci 46:971–981

Ridley JR, Diamond LW (2000) Fluid chemistry of lode-gold deposits and implications for genetic models. In: Hagemann SG, Brown P (eds), Gold in 2000. Rev Econ Geol 13: 141–162

Ridley JR, Hagemann SG (1999) Interpretation of post-entrapment fluid-inclusion re-equilibration at the Three Mile Hill, Marvel Loch and Griffins Find high-temperature lode-gold deposits, Yilgarn Craton, Western Australia. Chem Geol 154:257–278

Rubin JN, Kyle JR (1998) The Gunung Bijih Timur (Ertsberg East) skarn complex, Irian Jaya, Indonesia: Geology and genesis of a large, magnesian, Cu-Au skarn. In: Lentz DR (ed) Mineralized intrusion-related skarn systems. Min Ass Canada, Short Course 26: 245–288

Shenton S (2013) Locality 4: the geological setting of the Marvel Loch gold mine. In: Doublier MP (ed) Geological setting of mineral deposits in the Southern Cross district – A field guide. Geol Surv Western Australia Rec 2013/11: 37–40

Shimazaki H, Shimizu M, Nakano T (1986) Carbon and oxygen isotopes of calcites from Japanese skarn deposits. Geochem J 20:297–310

Simpson ES (1952) Minerals of Western Australia, Vol 1–3. Hesperian Press, Perth

Slyth P, Schwebel PJ (1995) Jaccoletti Zone One gold deposit. In: Schwebel PJ (ed) Southern Cross greenstone belt, geology and gold mines, pp. 91–95. Nedlands, Geoconferences Inc

Smirnov VI (1976) Geology of mineral deposits. MIR Publishers, Moscow

Soares GAR, Figueiredo e Silva RC, Hagemann SG, Lobato LM, Lucena RA, Lana CC (2025) Geologic setting and hydrothermal alteration at the Tucano gold deposit in northern Brazil: Evidence for a hypozonal orogenic gold system in the Guiana Shield. Econ Geol 120:275–306

Spear FS (1993) Metamorphic phase equilibria and pressure-temperature-time paths. Mineral Soc Am Monogr : 1–799

Sweetapple MT, Vanstone PJ, Lumpkin GR, Collins LF (2024) A review of lithogeochemical dispersion haloes of LCT pegmatites, and their application to rare metal exploration, with special reference to lithium in an Australian context. Austr J Earth Sci. https://doi.org/10.1080/08120099.2024.2379834

Thebaud N, Mole DM, Wingate MTD, Kirkland CL, Doublier MP (2013a) 205916: metasyenogranite, Withers Find road. Geol Surv West Australia. Geochronology Record 1121

Thebaud N, Wingate MTD, Kirkland CL, Doublier MP (2013b) 205912: granodiorite gneiss, Lake Julia. Geol Surv West Australia. Geochronology Record 1114

Thern ER, Nelson DR (2012) Detrital zircon age structure within ca. 3 Ga metasedimentary rocks, Yilgarn Craton: Elucidation of Hadean source terranes by principal component analysis. Precambrian Res 214–215:28–43

Tooth B, Ciobanu CL, Green L, O'Neill B, Brugger J (2011) Bi-melt formation and gold scavenging from hydrothermal fluids: An experimantal study. Geochim Cosmochim Acta 75:5423–5443

Watkins KP, Hickman AH (1990) Geological evolution and mineralization of the Murchison Province, Western Australia. Geol Surv West Australia Bull 137:1–267

Wells MA, Aylmore MG, McInnes BIA, Rickard WDA, Rankenburg K (2025) Mineral-textural characteristics of lithium pegmatite ores of Western Australia. Econ Geol 120:1287–1310

Whitney DL, Evans BW (2010) Abbreviations for names of rock-forming minerals. Am Mineral 95:185–187

Willett G (1973) Mafic and ultramafic rocks of the Lake Johnston and Marvel Loch areas, Western Australia. Unpublished M.Sc. thesis, University of Sydney

Williamson HC, Barr DJ (1965) Gold mineralization in the Yilgarn goldfield. In: McAndrew J (ed) Geology of Australian ore deposits. 8th Commonwealth Mining and Metallurgical Congress, Australia and New Zealand, 87–94

Wingate MTD, Kirkland CL, Doublier MP (2012) 199043: metamonzogranite dyke, Marvel Loch. Geol Surv Western Australia. Geochronology Rec 1076

Witt WK, Drabble M, Bodycoat FM (2001) Yilgarn Star gold deposit, Southern Cross greenstone belt, Western Australia: geological setting and characteristics of an amphibolite-facies orogenic gold deposit. Geol Surv Western Australia Rec 2001/17:45–62

Wu C-M, Chen H-X (2015) Revised Ti-in-biotite geothermometer for ilmenite- and rutile-bearing crustal metapelites. Sci Bull 60:116–121